Systematic Studies on Radio Emission of Extensive Air Showers with CoREAS and ZHAireS Simulations

Der Fakultät Mathematik und Naturwissenschaften, Fachgruppe Physik, der
Bergischen Universität Wuppertal zur Erlangung des akademischen Grades
Master of Science vorgelegte Arbeit

von

Marvin Gottowik

Referees: Prof. Dr. Karl-Heinz Kampert
Prof. Dr. Francesco Knechtli

Contents

1 Introduction

Although ultra high energy cosmic rays (UHECR) are the most energetic particles known so far fundamental questions as their origin and the acceleration processes are still unknown. At the highest energies the flux is typically in the order of one particle per year and square kilometer and lower. Thus, huge detectors like the Pierre Auger Observatory in Argentina are needed to detected a decent number of events.

When UHECR interact with the Earth‘s atmosphere an extensive air shower (EAS) is produced. Several methods are feasible and already used at the Pierre Auger Observatory to detect such an EAS. Typically the footprint of the shower, i.e. the particles which reach the ground, can be measured by a surface detector. Additionally the longitudinal profile can be analyzed using the emitted fluorescence light. A recent method is via its radio emission.

In this thesis the correlation of radiation energy and the primary energy is studied in detail. Therefore, lots of showers are simulated by CORSIKA and Aires with enabled computation of radio emission. Correcting the emitted radiation energy for several effects as shower direction and position of the shower maximum a dependency on the electromagnetic component of the shower is found which can be used to determine the energy scale.

To reconstruct the primary energy in an experiment the lateral distribution function is fitted to the data. The parameters of the LDF are correlated which allows to reduce the number of free parameters and replace them with constants. A cross check is performed with CORSIKA and Aires simulations to validate the estimation of the found constants.

This thesis is structured as follows. In chapter 1 a short introduction to cosmic rays and extensive air showers, the radio emission processes, current radio experiments and the used software is given. Chapter 2 describes the used model for an efficient computation of the radiation energy. The influence of the technical parameters in the simulations are discussed in chapter 3. In chapter 4 and 5 the radiation energy is studied for different scaling of the refractive index. Chapter 6 presents the cross check for the fit of the LDF. Finally, chapter 7 will summarize this thesis and present its conclusions.

1.1 Cosmic Rays and Extensive Air Showers

Cosmic rays are particles from outside our solar system with a wide range in energy up to 10^{20} eV and flux spanning more than 30 orders of magnitudes. Sources and mechanism for the acceleration of the particle to such energies are still unclear. An

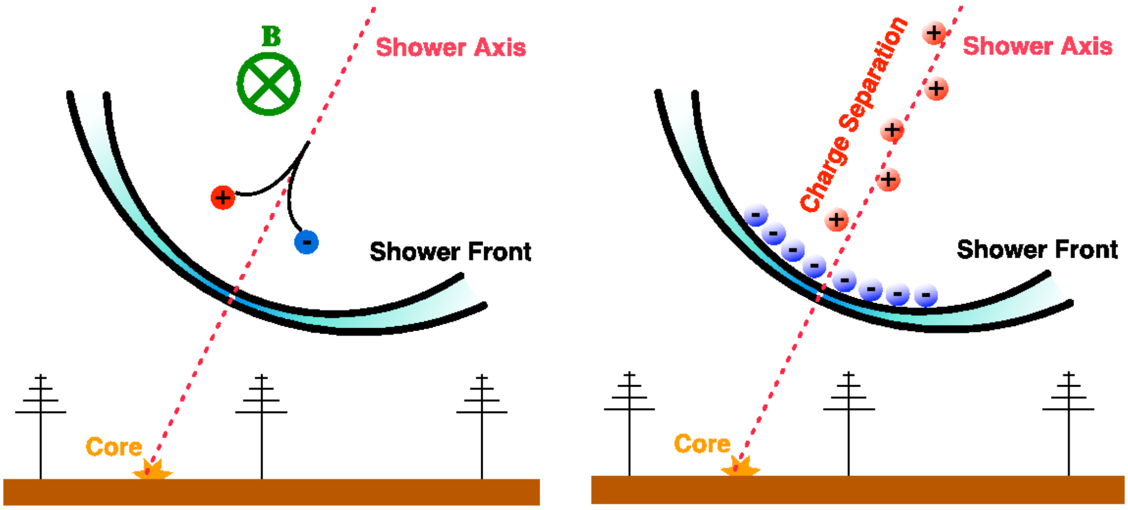

Figure 1.1: Sketch of the two emission processes of an air shower. The left plot shows the geomagnetic emission, the charge excess is shown by the right one. [1] and K.D. de Vries.

interaction of a high energy cosmic ray primary particle with an atmospheric nucleus initiates a cascade of secondary particles, the EAS.

In this first interaction high energy secondary particles are created which themselves will interact again with other nucleus in the atmosphere or decay after their lifetime in case of unstable particles and initiate further sub-cascades. This process continues until the energies are too low for further interactions or the particle reaches the ground.

The shower can be decomposed in three main components. The electromagnetic part ($e^{\pm}$, γ) contains approximately 95 % of the primary energy, the muonic part ($\mu^{\pm}$) carries about 4 % and the hadronic part (mostly pions) 1 %. Moving through the atmosphere the EAS produces radio emission which allows to observe the air shower developing in the atmosphere.

1.2 Radio Emission and Detectors

An EAS emits radio signals due to two different effects, the geomagnetic emission and the charge excess. Both are shown in figure 1.1.

The Lorentz force acts on the charged particles of an EAS while they are moving through the magnetic field of the earth. The positive and negative charges are deflected which leads to synchrotron like radio emission. The emitted radio signal is polarized in the direction of the Lorentz force, i.e. in $\vec{v} \times \vec{B}$ direction.

The second effect is based on a negative charge excess in the shower front due to knocked out electrons from the air molecules and annihilated positrons in the shower front. This allows an air shower to emit Cherenkov radiation at radio wavelengths with an radial polarization towards the shower core.

The radio signal is the superposition of both effects. Due to constructive and destructive interference of the emission the profile is asymmetric. The radio emission from EAS is strongest below 100 MHz, typically a frequency band between 30 to 80 MHz is used in an experiment.

Important radio detectors in a chronological order are LOPES [2], CODALEMA [3], the Pierre Auger Observatory [4], LOFAR [5] and Tunka-Rex [6]. Some of them are briefly described in the following. They differ in their general design and are exposed to different environmental circumstances. Thus, they complement each other and can be used for the verification of experimental results.

The Pierre Auger Observatory in Argentina is designed as a hybrid detector that can measures an air shower with a surface detector and the fluorescence light. In 2010 the Pierre Auger Observatory was extended by the Auger Engineering Radio Array (AERA) [7] to detect the radio signal, prototype stations are taking data since 2006. The antennas are placed on a regular grid with different spacings for the different stages of construction covering in total around 20 km^2. Due to the hybrid design correlations of the various shower components can be studied.

The next experiment, LOFAR , started its operation in June 2010. It consists of more than 20 000 antennas that are spread over several different countries in Europe. The density of antennas increases toward the center in the Netherlands. Here about 2400 antennas are clustered on an area of approximately 10 km^2. This allows to measure the radio signal with high precision.

The latest experiment is Tunka-Rex located in Siberia. It started operation in October 2012 with 12 antennas and has currently 63 antennas.

1.3 Simulation Software

For the simulation of the air showers two different programs CORSIKA 7.4100 [8] and Aires 2.8.4a [9] are used. For the computation of the radio emission the extension CoREAS [10] and ZHAireS [11] are enabled. The similarities and differences of the simulations are briefly explained in the following.

For the simulation of the air shower itself the primary particle is inserted in the top of the atmosphere. The point of interaction or decay is computed following a certain probability function. The first process is then performed and the secondary particles are sampled accordingly. Energy and momentum of the secondary particle are chosen randomly from a probability function such that the conversation laws hold. This process continues repeatedly until the particles energy is lower than some threshold, the particle is out of the region of interest or it reaches the ground level. During the propagation the radiation of the particles are calculated by the extensions CoREAS or ZHAireS respectively.

Both have in common that no assumption on the actual radio emission mechanism are made. The radiation is calculated by pure electrodynamics applied to each particle in the simulation. However, the used formalism differs. In CoREAS the “endpoint formalism” is used, whereas in ZHAireS implements the “ZHS Algorithm”. The difference in the calculation of the radio emission and the influence on the results are the main reason for this thesis. In Aires SIBYLL 2.1 is used as the high energy hadronic model. For a better comparison of the radio emission the same model is used in CORSIKA. Therefore, the old version 7.4100 has to be used because newer versions of CORSIKA do not support SIBYLL 2.1 anymore.

The earth curvature is taken into account in both programs. The air density in the atmosphere is implemented as a five layer model. The atmosphere is build-up of five spherically symmetric layer whose internal radius is the Earth's radius. The parameters of the model are obtained by a fit to the air density of the US standard atmosphere. The resulting model is called Linsley's parameterization and is used in both codes. Another difference is the default scaling of the refractive index n. For CoREAS n scales proportional to the gradient of the air density. In Aires a simple exponential scaling of n is used. The n scaling is expected to be a crucial point for the radio emission. To avoid effects of the refractive index in the comparison, first a constant index of $n = 1$ is used which is optionally available in both codes. Later the CoREAS code has been modified to use an Aires-like simple exponential n model for the refractive index. Comparisons with this modified version of CORSIKA will be shown as well. The refractivity at sea level will usually be set to $n - 1 = 2.92 \times 10^{-4}$.

The used coordinate systems are also different. Throughout this thesis all angles are given in the Auger definition. A zenith angle of 0° means a vertical shower, for higher zenith angles up to 90° the shower gets more horizontal. For the azimuth angle 0° points in east direction proceeding counterclockwise, e.g. south corresponds to an azimuth angle of 270°.

2 Model

The model used for an efficient extraction of the radiation energy is presented in this chapter. This method was first introduced in [12], studies with CORSIKA simulations were already done there. One of the main tasks of the following chapters will be to validate this results with Aires simulations. The accuracy of the method is analyzed for both programs independently and the individual steps in the analysis of the simulation output are explained.

2.1 Calculation of the Radiation Energy

For an efficient determination of the radiation energy only a small number of antennas is enough if they are placed in a very specific way. The computing time increases with the number of simulated antennas. Thus, it is unfeasible to place lots of antennas to sample the full two dimensional emission pattern.

Using the fact that the electric field has no contribution in the direction of propagation it is sufficient to study the perpendicular plane, the so called shower plane. It is convenient to chose the axes in $\vec{v} \times \vec{B}$ and $\vec{v} \times (\vec{v} \times \vec{B})$ direction. Looking at the polarization pattern of the geomagnetic emission and the charge excess one can see that they now decouple on the $\vec{v} \times (\vec{v} \times \vec{B})$ axis. Hence they can be studied independently at each antenna position.

Assuming that the geomagnetic and charge excess components are in phase and their respective lateral distribution functions (LDF) are radially symmetric it follows that the radiation energy can be computed via

$$E_{\mathrm{RD}} = 2\pi \int_0^\infty \mathrm{d}r \, r \; f(r, \phi = 90^\circ). \tag{2.1}$$

Thus only the $\vec{v} \times (\vec{v} \times \vec{B})$ is needed for the calculation of the radiation energy. This reduces the number of antennas and therefore the computing time of a simulation a lot. In the following, 30 antennas are placed on the $\vec{v} \times (\vec{v} \times \vec{B})$ axis such that the complete radio footprint is covered. The first antenna is placed at 5 ‰ of the size of the radio footprint. The next twelve antennas are equally spaced from 1 % to 15 %. The last 17 antennas are placed with an equal spacing from 20 % until the maximal size of the radio footprint. The spacing is denser close to the shower core to detect a possible rapid change of the energy fluence and to be sensitive for the different shapes of the lateral distribution function. For larger distances this is no longer necessary. Therefore it ensures an adequate sampling of the radio LDF, such that the uncertainty of the numerical integration can be neglected. This setup is sketched in figure 2.1.

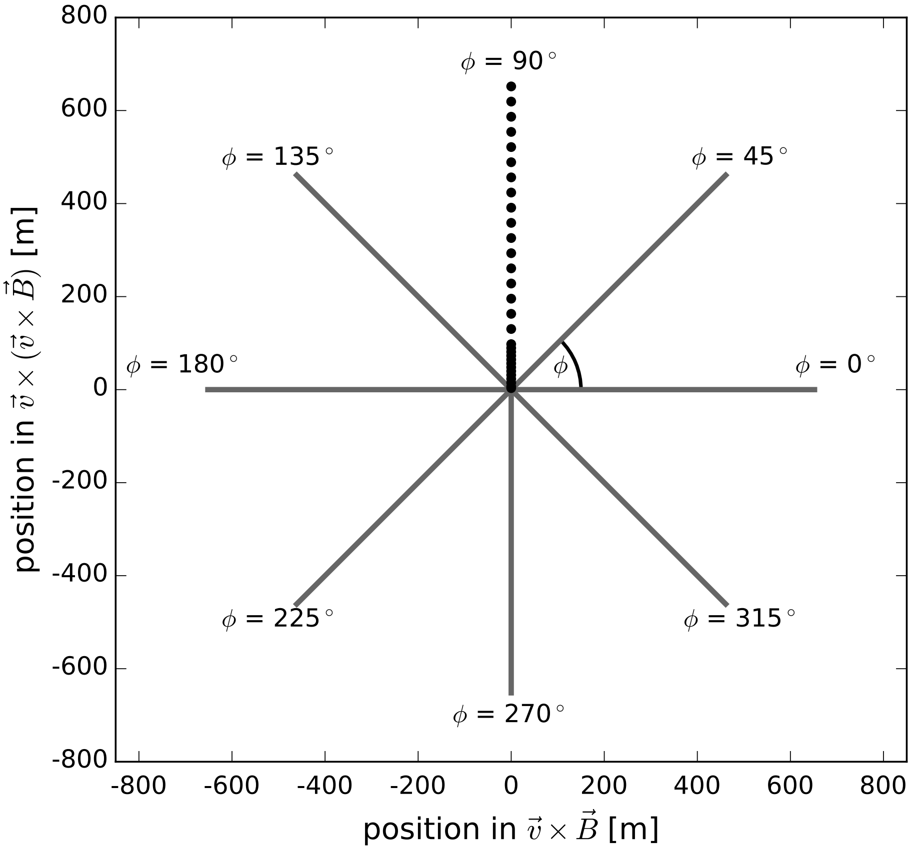

Figure 2.1: Sketch of the positions of the antennas in the shower plane. On the $\phi = 90°$ axis each circle corresponds to an antenna position.[12]

As the radiation is almost solely emitted by the electromagnetic part of the air shower it correlates best with the energy of the electromagnetic cascade. Due to the much lower charge to mass ratio muons hardly emit radiation and can be neglected. A method to express the invisible energy as a function of the electromagnetic energy is presented in [13]. Combining both allows to compute the primary energy from the radiated energy of the electromagnetic cascade.

2.2 Analysis Steps

The individual steps in the analysis of the simulation output are explained and depicted in figure 2.2. The simulation yields the three dimensional electric field traces of each antenna in the used carthesian coordinate system of the program. The traces are Fourier transformed and bandpass filtered to 30 to 80 MHz. This is the frequency band which is mostly used in experiments.

The filtered traces are then transformed back to the time domain. Due to the bandpass the trace contains oscillations which extends the pulse to the end of the

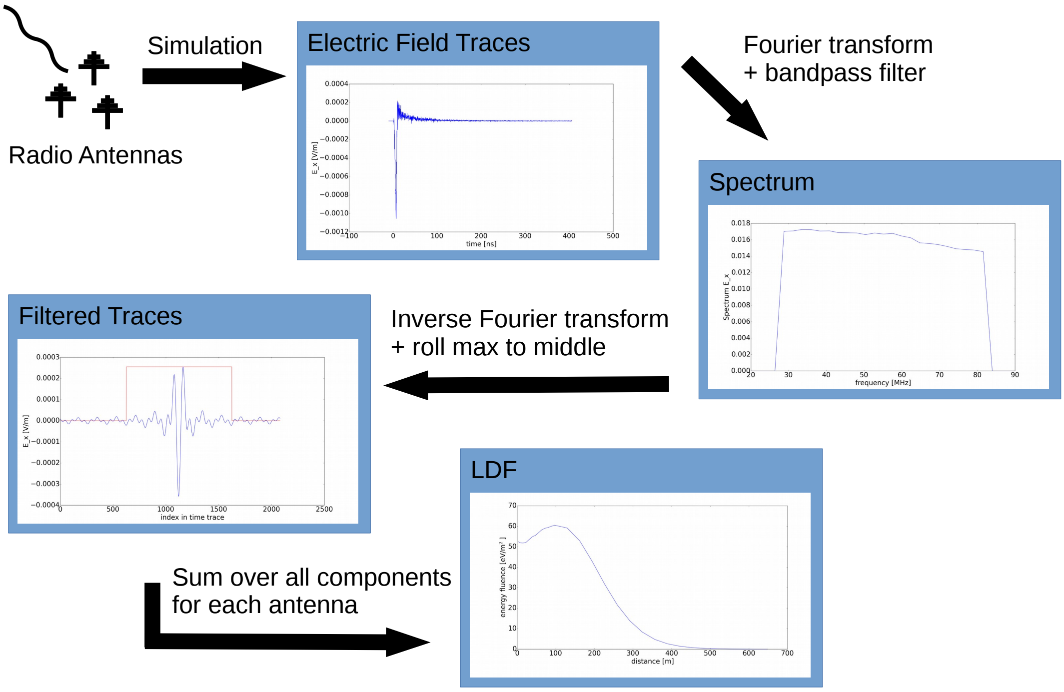

Figure 2.2: Sketch of the steps from the incoming electric field to the LDF in the analysis of the simulation output.

trace. The trace is now shifted such that the maximum of the Hilbert envelope is in the middle of the trace. A time window of 200 ns centered at the maximum is used to determine the signal range. The electric field outside of the time window is treated as noise and used to estimate the noise in the signal range. The remaining energy of the electric field is therefore the actual signal. Since this is a Monte Carlo study with an ideal detector there is no real noise on the traces. However, this procedure is used to be consistent with an experimental setup.

Summing up all components of the electric field the energy fluence at this station can be computed. Plotting this against the distance from the core in the shower plane yields the LDF. An integration according to equation 2.1 provides the radiation energy.

2.3 Accuracy of the method

In the following, the impact of the used assumptions and the reduction on the $\vec{v} \times (\vec{v} \times \vec{B})$ axis is studied. Therefore, 250 air showers with a primary energy between 10^{17} to 10^{19} eV according to a uniform distribution of the logarithm of the energy are simulated. The azimuth angle is distributed uniformly between 0 to 360° and the zenith angle

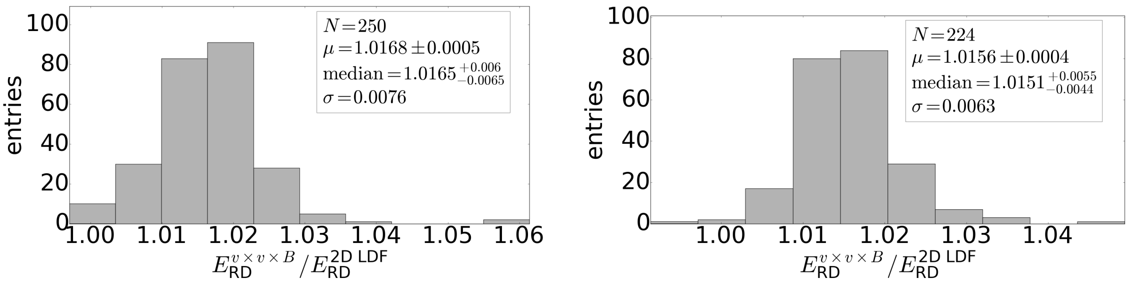

Figure 2.3: Comparison of the emitted radiation energy using only the positive $\vec{v} \times (\vec{v} \times \vec{B})$ arm and sampling the shower plane with a star shape pattern. Shown is the ratio of 250 air showers for CoREAS (left) and 224 showers for ZHAireS (right).

uniformly in 0 to 75°. The geomagnetic field is set to an inclination of $-35.7°$ with an field strength of 0.243 G which corresponds to the geomagnetic field at the AERA detector. In the following this setup will be denoted by “random showers”. Due to hardware or network failures not all started simulations have finished successfully. Hence, the number of data points can differ slightly for the plots in the following.

The radio antennas are placed in a star shape pattern, i.e. in 45° lines, in the shower plane using the same distribution as explained in the previous section. For ZHAireS the spacing has to be increased a little as the total number of antennas is limited to 200. Thus only 25 antennas instead of 30 can be placed for each direction.

The star data is interpolated and integrated numerically over the complete shower plane to compute E_{RD} from the two dimensional LDF. Additionally it is computed using the $\vec{v} \times (\vec{v} \times \vec{B})$ axis only. Their ratios are shown in figure 2.3 for CoREAS and ZHAireS. An overestimation of 1.68 % (1.56 %) is found for CoREAS (ZHAireS). The bias can be attributed to the two assumptions made as described in [12]. To corrected this bias E_{RD} will be reduced accordingly for the following analysis.

3 Simulation Parameters

In a shower simulation several technical parameters are involved which can have a physical influence. An important one is the thinning algorithm which is used to reduce the number of tracked particles and therefore speed up the simulation. Also the hadronic interaction model can influence the shower development. Therefore, SIBYLL 2.1 [14] is used in both program to treat high energy hadronic interactions. In CORSIKA also a low energy hadronic model can be specified. Here two famous models, FLUKA [15] and UrQMD [16], are compared. All other parameters like low energy cuts for the different particle species are set to the same value if possible. For this analysis the refractive index is set to 1.

3.1 Thinning Algorithm

The number of secondary particles in an air shower depends strongly on the cosmic ray energy. For a 10^{20} eV proton primary an air shower contains typically around 10^{11} particles which make it practically impossible to follow them all in the simulation. Hence thinning algorithms are used to reduce the number of tracked particles without changing the shower development. In this section the dependency of the radiation energy on the thinning level is analyzed.

In CORSIKA one can specify the thinning level as a fraction of the primary energy, i.e. $\varepsilon_{\mathrm{thin}} = E/E_0$. If the sum of the energy of all secondary particles in an interaction is lower than the thinning energy only one particle of that interaction is followed. The followed particle gets a weighting factor such that the total energy is conserved. To analyze the influence of this thinning several proton shower with 1 EeV primary energy, 50° zenith angle and 270° azimuth angle are simulated for different thinning energies.

Table 3.1: Radiation energy of an air shower depending on the used thinning level in CORSIKA. The shower is induced by a proton with 1 EeV primary energy and fixed geometry of 50° zenith angle coming from the south. The refractive index is set to 1.

thinning level	radiation energy/MeV	number of simulations
10^{-3}	10.2 ± 0.2	40
10^{-4}	8.5 ± 0.1	40
10^{-5}	8.3 ± 0.1	40
10^{-6}	8.3 ± 0.1	40
10^{-7}	8.4 ± 0.1	21

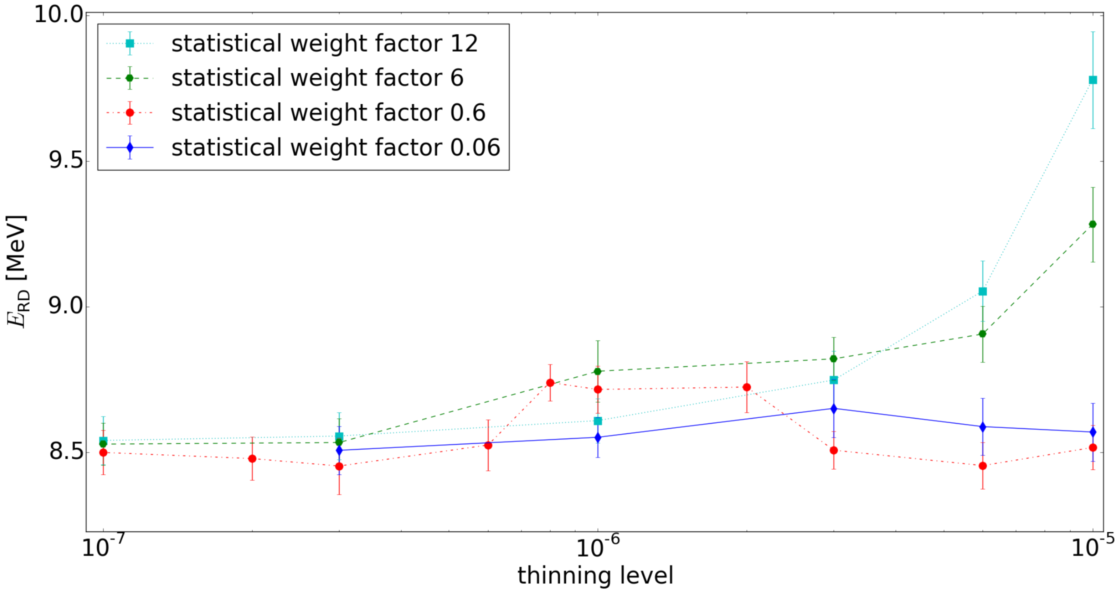

Figure 3.1: Radiation energy of an air shower depending on the Aires thinning parameters. The shower is induced by a proton with 1 EeV primary energy and fixed geometry of 50° zenith angle coming from the south. The refractive index is set to 1.

The direction is chosen because at the Pierre Auger Observatory most of the showers are expected from this direction. The resulting radiation energies are shown in table 3.1. For a lower thinning level less radiation energy is emitted. By approximating several low energetic particles with a single particle and a higher weight an artificial coherence is introduced in their radio emission. If the thinning process already starts at higher particle energies more radiation is emitted coherently. As there is no significant difference for thinning levels lower than 10^{-5} this one is used in the following to reduce computing time.

Thinning in Aires works similarly as in CORSIKA. In addition, one can specify a statistical weight factor to diminish statistical weight fluctuations. Again 40 showers with the same shower parameters as above are simulated for different combinations of both thinning parameters. The results are shown in figure 3.1. For the default value of the statistical weight factor (12) an exponential dependency on the thinning level can be seen. For a very low weight factor of 0.06 the total radiation energy is almost constant for all thinning level. The low weight factor is used to mimic a kind of sandwich thinning, i.e. to disable thinning of very high and low energetic particles [17]. In the following a thinning level of 10^{-5} with a weight factor of 0.06 is used for all ZHAireS simulations.

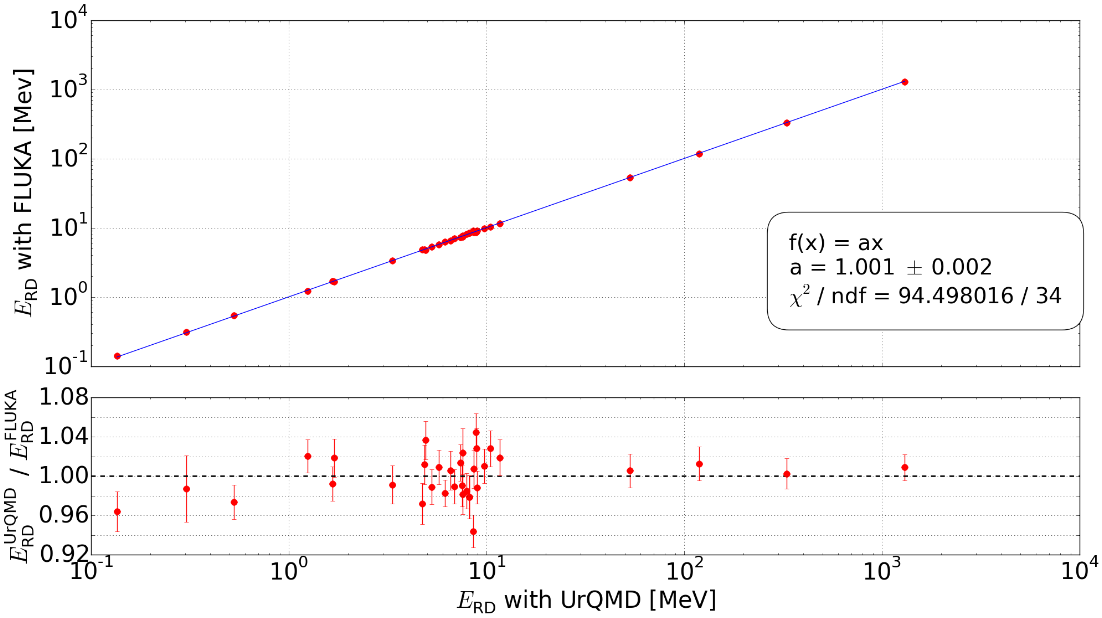

Figure 3.2: Comparison of the radiation energy using FLUKA and UrQMD. The showers are induced by a proton primary for different energies and angles. Each point contains 40 showers which differ only in the initial seed. The uncertainty are too small to be visible in the upper plot. In the lower plot the error bars are calculated using gaussian error propagation using the uncertainties of the mean.

3.2 Influence of the Low Energy Hadronic Model

To investigate the impact of the low energy hadronic model on the radiation energy several sets of air showers are simulated using the two models FLUKA and UrQMD. Each set consists of 40 proton induced showers which differ only in the initial seed. At first the dependence is studied differentially. Two of the physical quantities zenith, azimuth and energy are fixed while the third one varies. Later they are combined to quote the general influence.

Fixing the primary energy to 1 EeV and the zenith angle to 50° while the azimuth angle varies from 0° to 330° in 30° steps yields $(1 \pm 4)\,‰$ less radiation energy using FLUKA. However changing the azimuth angle has only an influence on the geomagnetic emission and does not change the shower development.

For a 1 EeV primary energy coming from the south with zenith angles from 0° to 75° in 5° steps $(1 \pm 3)\,‰$ more radiation is emitted using FLUKA.

Lastly the shower direction is fixed to an zenith angle of 50° coming from the south. For the primary energy the following values are used: 0.1 EeV, 0.2 EeV, 0.3 EeV, 0.5 EeV, 1 EeV, 2 EeV, 3 EeV, 5 EeV and 10 EeV. Now $(3 \pm 4)\,‰$ more radiation energy is observed if FLUKA is used. For a higher cosmic ray energy more low energetic hadrons are produced. However, they have only a small influence on the shower development. Hence, there is no dependency on the primary energy.

Figure 3.2 combines all data. The linear fit yields (1 ± 2) ‰ more radiation energy with FLUKA. One can conclude that the low energy hadron model has no influence for the desired accuracy of this study. If the intersection with the y axis is added to the fit the slope deviates from one by (-1 ± 2) ‰ and the offset is fitted to 0.006 ± 0.002. The results show no significant deviation and the precision of the test is better than the usual uncertainties in the following analysis, which are on a percentage level. As the choice has no significant influence on the analysis, UrQMD is used for convenience.

4 Constant Refractive Index of the Atmosphere

In this chapter the necessary steps for the correction of the radiation energy for shower parameters as incoming direction and X_{max} value are shown for a constant refractive index of one. Although this is highly nonphysical it is the only common setting that CoREAS and ZHAireS can simulate directly. But here only the consistency between both programs will be studied. However, this yields much less radiation energy compared to a more physical scaling of the refractive index.

4.1 Charge Excess Fraction

An important point in the analysis of the radio signal is the determination of the charge excess fraction a. This ratio obviously depends on the geomagnetic angle, i.e. the angle between magnetic field and shower direction, α. One can generalize the definition to

$$a = \sin(\alpha)\sqrt{E_{\mathrm{RD}}^{\mathrm{ce}}/E_{\mathrm{RD}}^{\mathrm{geo}}}. \tag{4.1}$$

The square root is taken for consistency with previous work where the electric field amplitude was used instead of the radiation energy. Since the used method allows to decompose the radiation energy into a geomagnetic and a charge excess part a can be studied directly.

500 proton induced random showers are simulated. For each shower the radiation energy originating from the geomagnetic emission and the charge excess is calculated independently. Figure 4.1 shows the resulting charge excess fractions. One can see that a is not a constant. As most radiation is emitted close to the shower maximum X_{max} the air density $\rho \equiv \rho(X_{\mathrm{max}})$ at that height is used to parametrize the dependency. Using the US standard atmosphere after Linsley ρ can be calculated directly from X_{max} and the zenith angle θ.

An exponential function of the form

$$a(\rho) = q_0 + q_1 \cdot \exp\left(q_2(\rho - \langle\rho\rangle)\right) \tag{4.2}$$

is fitted to the data. $\langle\rho\rangle = 0.65\,\mathrm{kg\,m^{-2}}$ is the air density at the shower maximum for an average zenith angle of 45° and an average $\langle X_{\mathrm{max}}\rangle = 669\,\mathrm{g\,cm^{-3}}$ as predicted by QGSJETII-04 for a shower energy of 1 EeV and a 50 % proton/50 % iron composition [18]. The color code indicates that most outliers are air showers with a small $\sin(\alpha)$ value. The results of the fit are also given in figure 4.1. The optimal fit values for CoREAS and ZHAireS show a good agreement. The only significant deviation is found

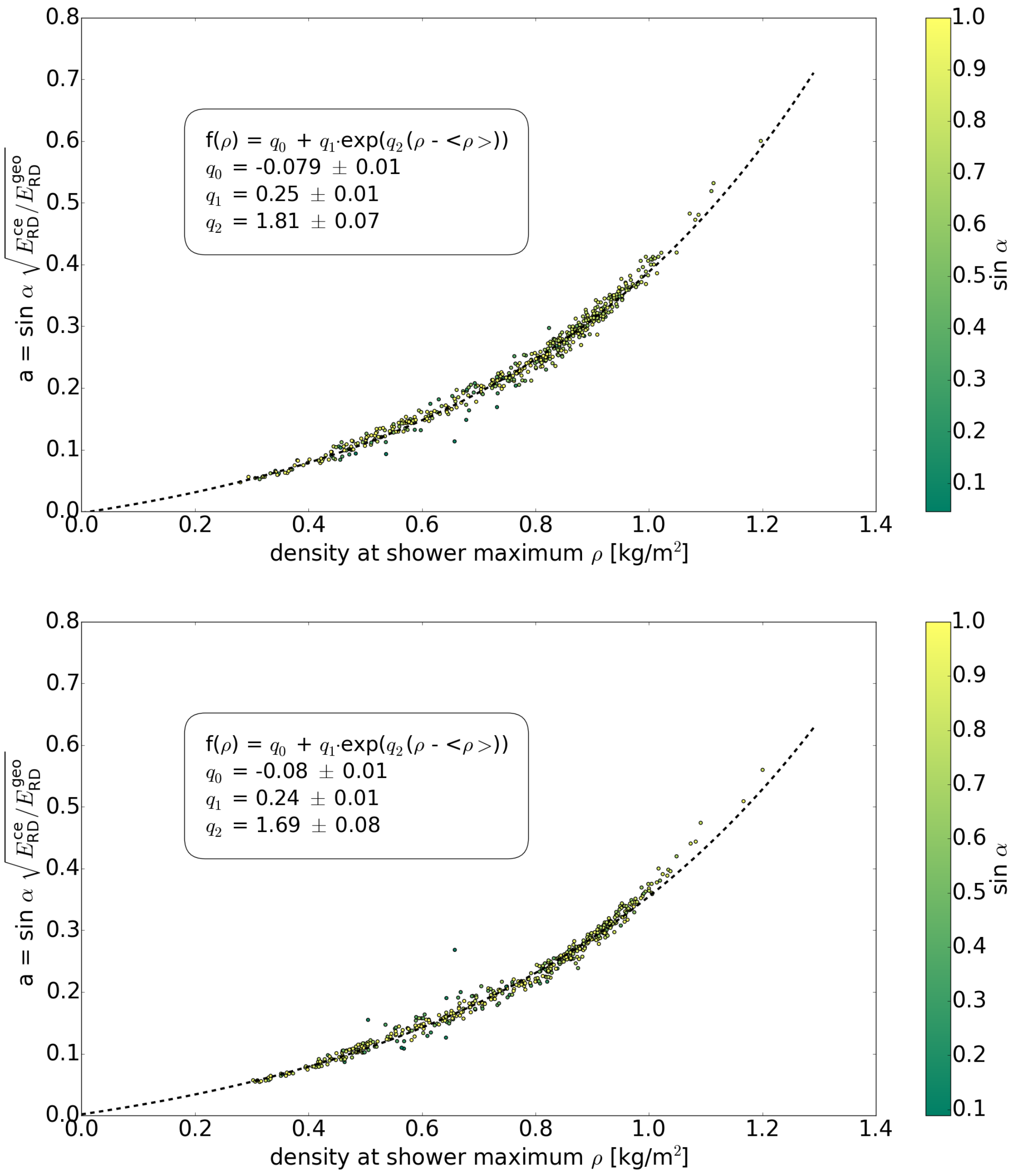

Figure 4.1: Charge excess fraction a of an air shower depending on the atmospheric density at the shower maximum for CoREAS (top) and ZHAireS (bottom).

in the parameter q_2. This has an influence only at large densities. This can be seen in direct comparison of the data in figure 4.2 that shows a small difference for air showers with a higher X_{max} value.

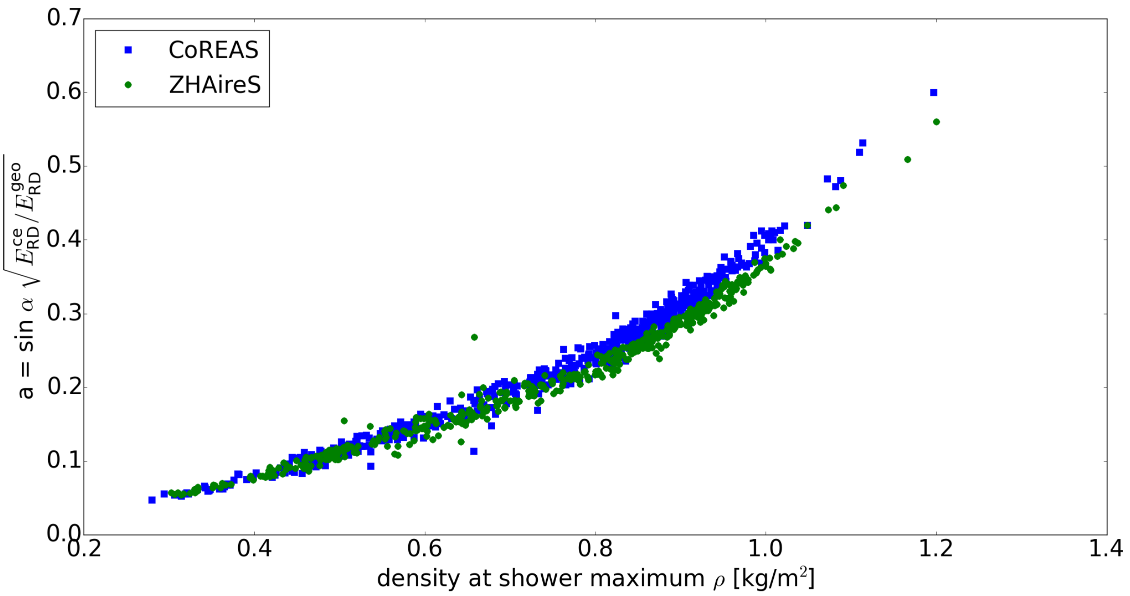

Figure 4.2: Direct comparison of the charge excess fraction for CoREAS and ZHAireS simulations depending on the atmospheric density at the shower maximum.

4.2 Corrected Radiation Energy

To correlate the radiation energy with the electromagnetic energy two corrections have to be applied. The geomagnetic part of the radiation energy depends on the magnetic field strength B and the geomagnetic angle α and scales with $\sin^2\alpha$. The dependency on the magnetic field is not taken into account now because all showers are simulated using the same magnetic field at the Pierre Auger Observatory. Thus, only the geomagnetic part has to be corrected for the geomagnetic angle which yields the first corrected radiation energy

$$S_{\mathrm{RD}}^{*} = \frac{E_{\mathrm{RD}}}{a(\rho)^2 + (1 - a(\rho)^2)\sin^2\alpha}. \tag{4.3}$$

An additional correction arise due to the air shower developing according to the slant depth whereas the radiation energy increases with the geometric path length of the shower development. For a lower atmospheric density the ratio between the geometric path length and propagation length measured in atmospheric depth is larger than for higher densities. Comparing two showers with the same primary energy, the one developing earlier in the atmosphere has a slightly larger radiation energy because the air gets more dense for an increasing atmospheric depth. Again, the density at the shower maximum ρ is used for the parametrization. Figure 4.3 shows the corrected radiation energy S_{RD}^{*} per electromagnetic energy E_{emag} as a function of ρ for several 1 EeV showers. An exponential function can be fitted to the data, the results are given in the figure. CoREAS and ZHAireS agree well within the given uncertainties.

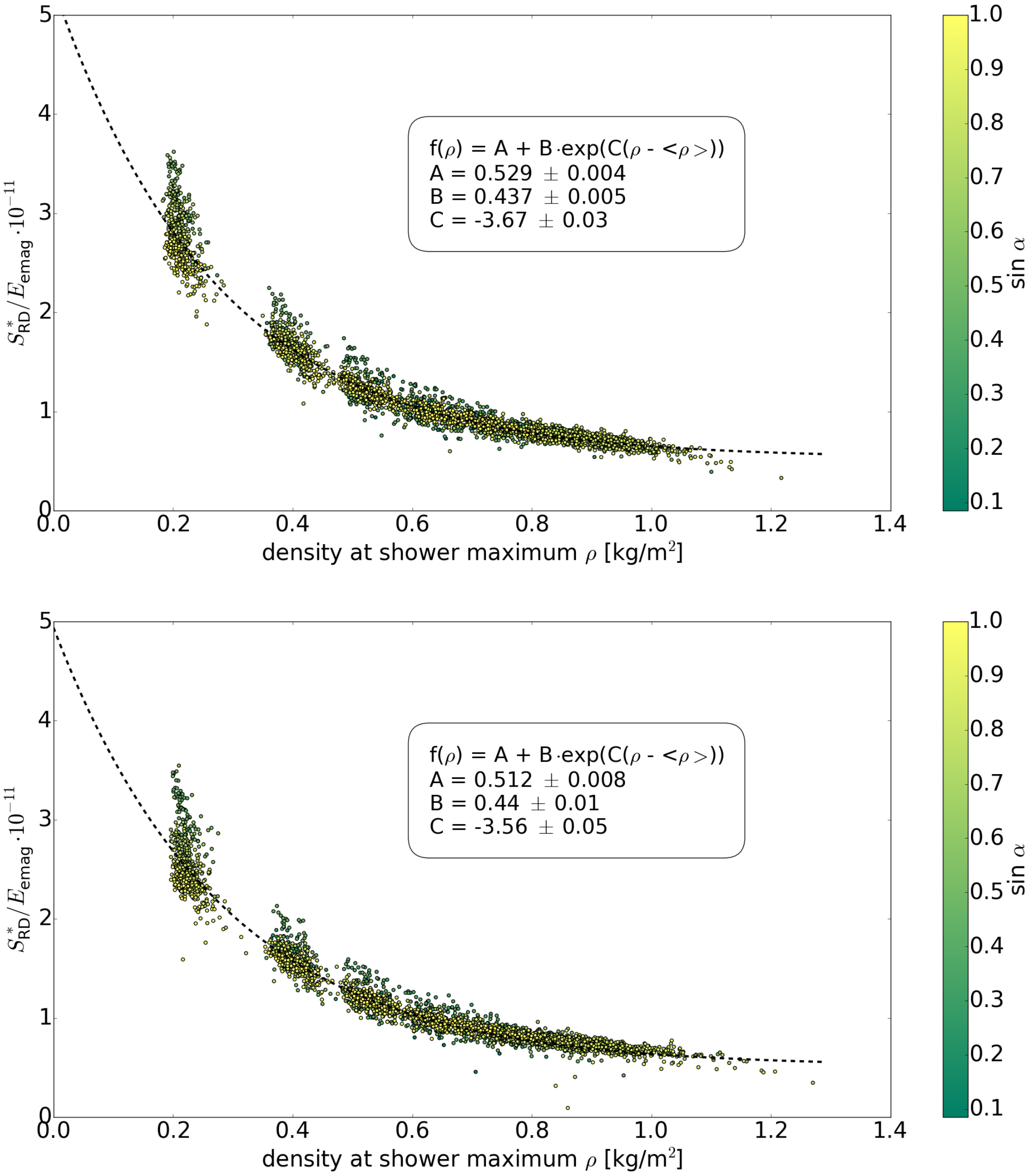

Figure 4.3: Corrected radiation energy relative to the energy in the electromagnetic part of the shower plotted as a function of the density at the shower maximum for CoREAS (top) and ZHAireS (bottom).

To add this dependence into the corrections, a second term with two free parameters p_0 and p_1 is added. The final corrected radiation energy is then given by

$$S_{\mathrm{RD}} = \frac{E_{\mathrm{RD}}}{a(\rho)^2 + (1 - a(\rho)^2)\sin^2\alpha} \cdot \frac{1}{(1 - p_0 + p_0 \exp\left[p_1(\rho - \langle\rho\rangle)\right])^2} \tag{4.4}$$

with ρ and $\langle\rho\rangle$ defined as mentioned above.

Table 4.1: Best fit parameters of equation (4.4) and (4.5) for CoREAS and ZHAireS using 500 proton induced random showers.

	CoREAS	ZHAireS
A	1.063 ± 0.006	1.046 ± 0.006
B	1.990 ± 0.003	1.992 ± 0.003
p_0	0.37 ± 0.02	0.31 ± 0.02
p_1	-2.3 ± 0.1	-2.5 ± 0.1

Table 4.2: Individual and combined parameters for the corrections of the radiation energy. The q_i values belong to the charge excess fraction, p_i are used in the second correction term.

	CoREAS	ZHAireS	combined
q_0	-0.08 ± 0.01	-0.08 ± 0.01	-0.08
q_1	0.25 ± 0.01	0.24 ± 0.01	0.245
q_2	1.81 ± 0.07	1.69 ± 0.08	1.76
p_0	0.37 ± 0.02	0.31 ± 0.02	0.34
p_1	-2.3 ± 0.1	-2.5 ± 0.1	-2.4

The free parameters p_0 and p_1 are determined in a combined fit with the power law

$$S_{\mathrm{RD}} = A \cdot 10^7\,\mathrm{eV}(E_{\mathrm{emag}}/10^{18}\,\mathrm{eV})^B. \tag{4.5}$$

The results are given in table 4.1. The value of $B \approx 2$ shows that S_{RD} scales quadratically with the electromagnetic energy. The correlations between the corrected radiation energy and the electromagnetic energy are shown in figure 4.4. Looking at the deviation of data and fit a scatter of roughly 7.5 % can be seen as shown in figure 4.5. This corresponds to an scatter of ≈ 3.8 % of the energy in the electromagnetic component.

Ignoring the slightly different optimal B values an estimate of the systematic uncertainty of the radiation energy is given by the ratio of $A_{\mathrm{CoREAS}}/A_{\mathrm{ZHAireS}} = 1.6\,\%$ which corresponds to a systematic uncertainty of 0.8 % for the electromagnetic energy. Nevertheless, the differences in the charge excess fraction are bigger.

To use this method for actual data a single set of correction parameters is needed. Hence the results of CoREAS and ZHAireS are combined. The individual and the combined parameters are summarized in table 4.2. Only for p_0 the combined parameter is not inside the uncertainty of the individual ones.

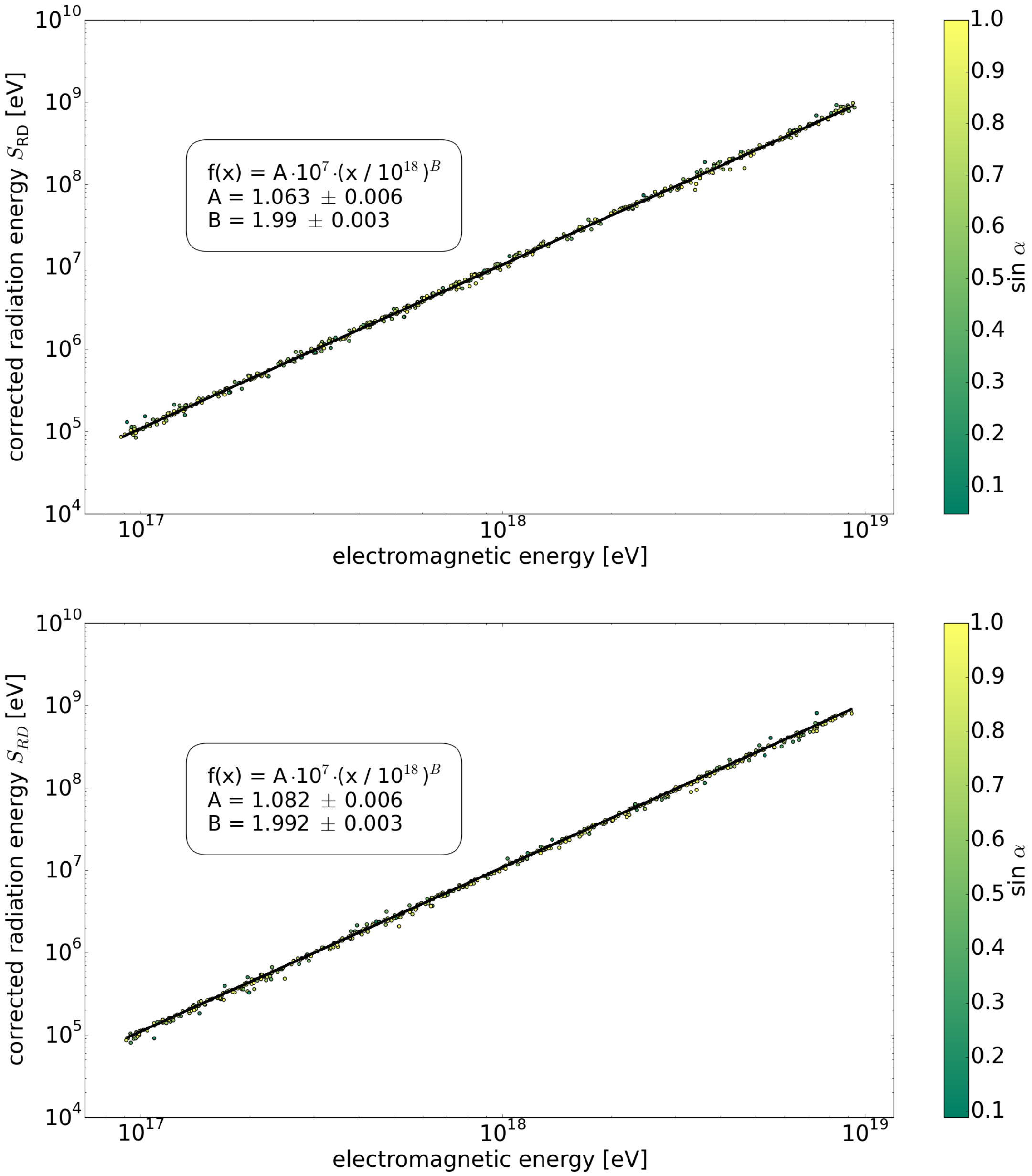

Figure 4.4: Correlation between the corrected radiation energy and the electromagnetic component of an air shower for CoREAS (top) and ZHAireS (bottom).

Redoing the power law fit yields slightly different results as shown in table 4.3. Using $A_{\mathrm{CoREAS}}/A_{\mathrm{ZHAireS}}$ again as an estimate for the systematic uncertainty it has increased to 3.8 %. As shown in figure 4.6 the scatter around the fit increased slightly. Comparing the corrected radiation energy with the combined corrections in figure 4.7 yields a good agreement.

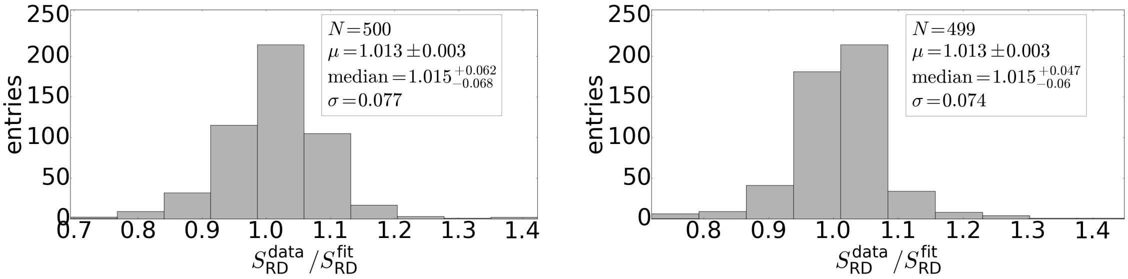

Figure 4.5: Scatter of the corrected radiation data and the fitted power law for CoREAS (left) and ZHAireS (right).

Table 4.3: Best fit parameters of equation (4.4) and (4.5) for CoREAS and ZHAireS with the combined corrections using 500 proton induced random showers.

	CoREAS	ZHAireS
A	1.081 ± 0.001	1.042 ± 0.001
B	1.989 ± 0.001	1.994 ± 0.001

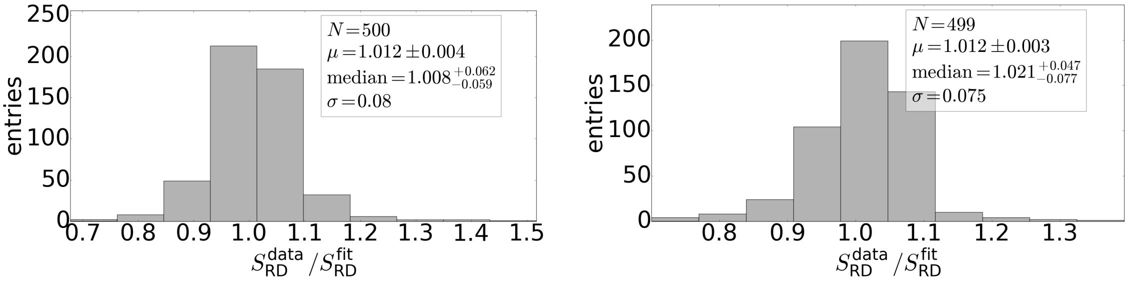

Figure 4.6: Scatter of the corrected radiation data using the combined corrections and the fitted power law for CoREAS (left) and ZHAireS (right).

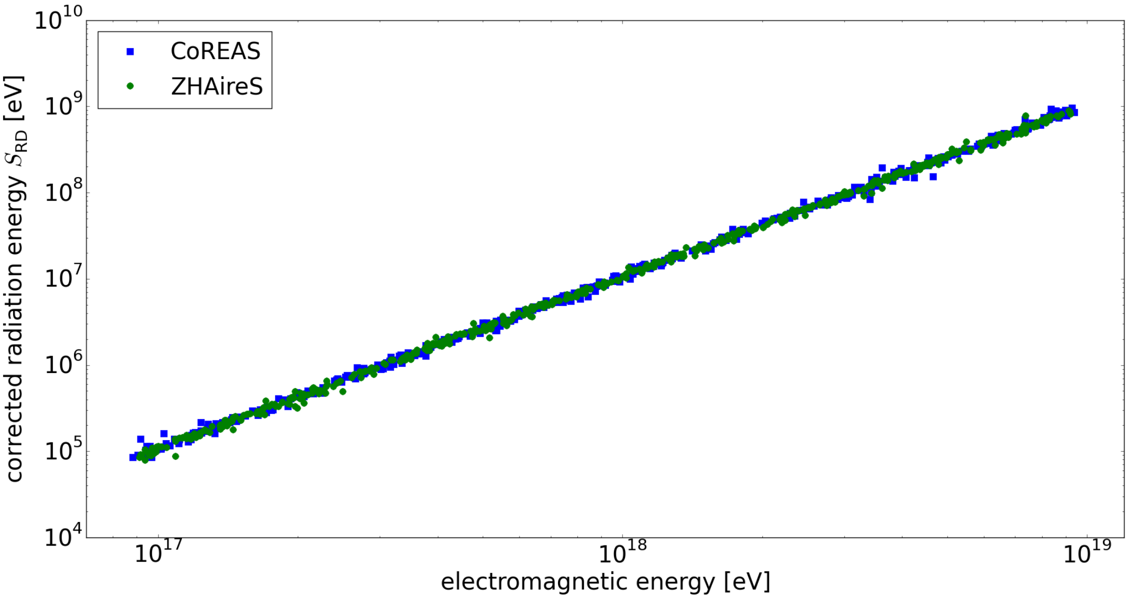

Figure 4.7: Direct comparison of the corrected radiation energy using the combined corrections for CoREAS and ZHAireS.

4.3 Detailed View at 1 EeV Showers

Since small differences are hardly visible in a log-log plot 40 proton induced air showers with a primary energy of 1 EeV are simulated for different shower directions each. The zenith angle is chosen in 10° steps from 10° to 80°, the azimuth angle is chosen in 30° steps from 0° to 360°. If several showers with the same setting are simulated S_{RD} is extended by an additional factor

$$S_{\mathrm{RD}} \propto \left(\frac{\langle E_{\mathrm{emag}} \rangle}{E_{\mathrm{emag}}}\right)^2 . \tag{4.6}$$

Due to random fluctuations each shower has a slightly different electromagnetic energy. With this normalization to the mean energy in the electromagnetic component the spread of S_{RD} is reduced. Thus, less simulations are needed for the same accuracy.

For each combination of azimuth and zenith angle the ratio of the radiation energy of CoREAS and ZHAireS is calculated. In figure 4.8 they are plotted against the zenith angle. A clear dependence of the ratio on the zenith angle can be seen. It is not understood where this dependency comes from.

Applying the individual corrections as presented in the previous section this dependence is overcorrected for small zenith angles. Although there is less radiation energy in CoREAS than in ZHAireS there is more corrected radiation energy. The results are shown in figure 4.9. The data is in agreement with a constant shift of 1 % of the corrected radiation energy in CoREAS.

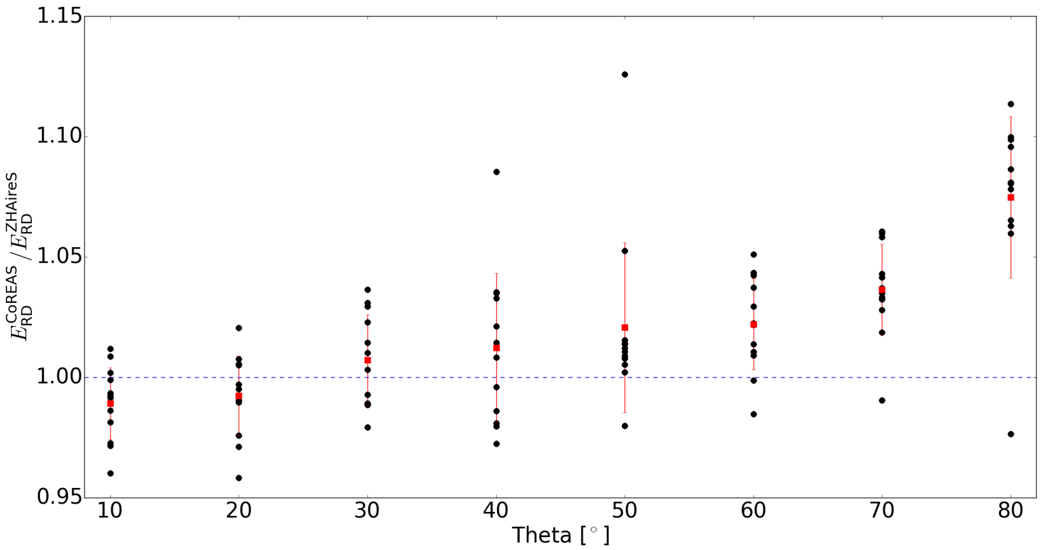

Figure 4.8: Ratio of the radiation energy of CoREAS and ZHAireS for different azimuth angles plotted against the zenith angle. In red the mean value and the standard deviation is shown.

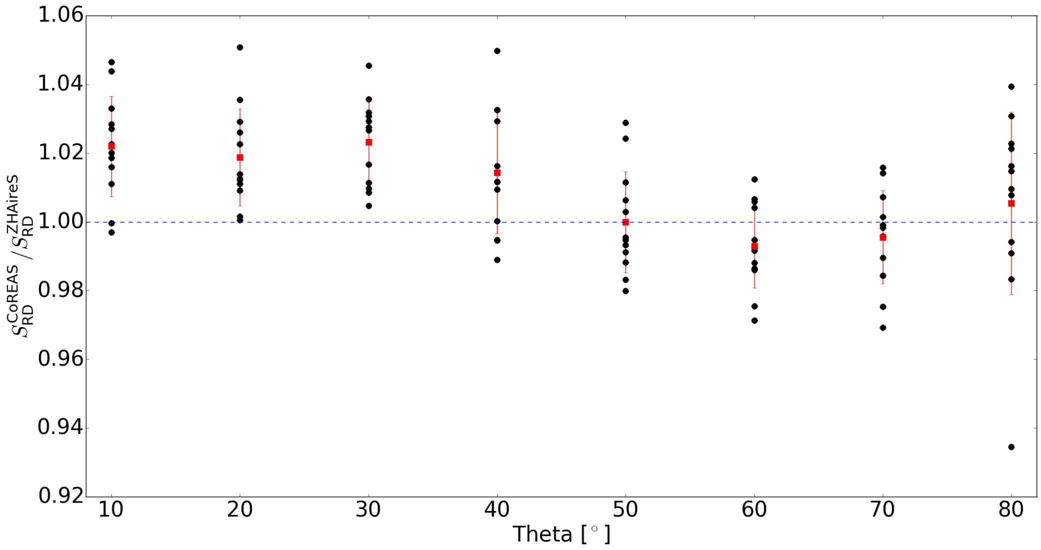

Figure 4.9: Ratio of the corrected radiation energy using the individual corrections of CoREAS and ZHAireS for different azimuth angles plotted against the zenith angle. In red the mean value and the standard deviation is shown.

However, using the individual corrections also corrects for the differences which should be analyzed. Correcting the radiation energy with the combined parameters yields figure 4.10. Again, there is a θ dependency. Comparing this with figure 4.8 one can see that the axis scale reduced roughly from $(-3, +10)\%$ to $(-2, +6)\%$.

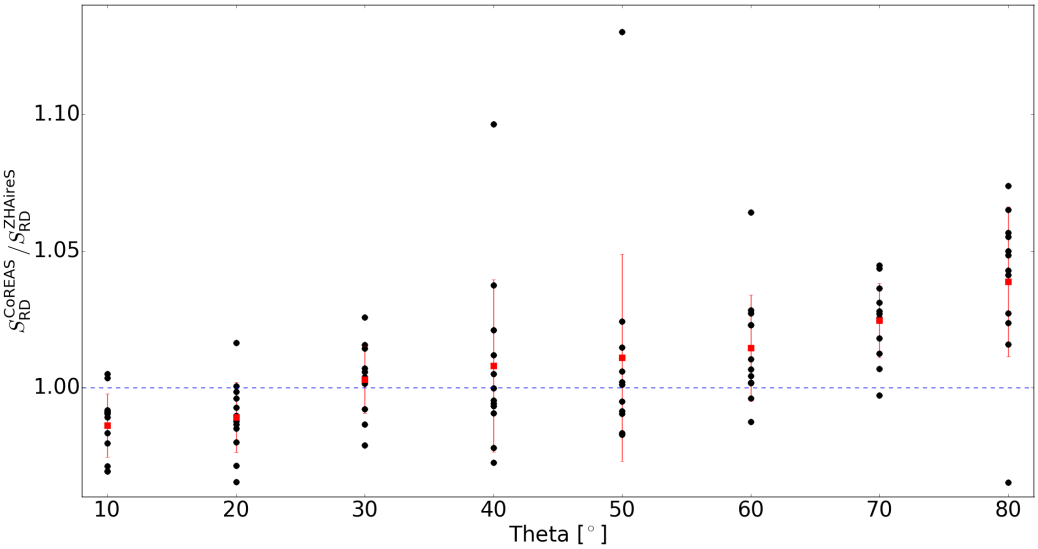

Figure 4.10: Ratio of the corrected radiation energy using the combined corrections of CoREAS and ZHAireS for different azimuth angles plotted against the zenith angle. In red the mean value and the standard deviation is shown.

5 Exponential Refractive Index of the Atmosphere

The comparison between CoREAS and ZHAireS are studied in this chapter using a modification to the CORSIKA code which allows to set the refractive index to an exponential scaling. This is more realistic than the constant refractive index, but not as good as the standard five layer model of CORSIKA. The correction steps described in the previous chapter are repeated. In section 5.3 1 EeV showers are studied in more details. The difference between proton and iron primaries is studied in section 5.4 and the effect of the refractive index is shown in section 5.5. The scaling with the magnetic field is analyzed section 5.6. The difference between having the antennas on the positive or negative $\vec{v} \times (\vec{v} \times \vec{B})$ arm is analyzed in section 5.7. In section 5.8 the corrections are repeated without knowing the X_{max} value as it would be the case for an real experiment.

5.1 Charge Excess Fraction

For the analysis of the charge excess fraction 1000 proton and 1000 iron induced random showers are simulated. The evaluation is done similar to section 4.1. Looking at the direct comparison first a deviation for showers with a high X_{max} value can be seen in figure 5.1 similar to figure 4.2.

An exponential function is fitted to the data. The results including the optimal fit parameters are shown in figure 5.2. Again one can see that only points with a small $\sin(\alpha)$ value deviate from the fit.

5.2 Corrected Radiation Energy

The determination of the parameters for the correction of the radiation energy is done as in the previous chapter. The results are given in table 5.1 and shown in figure 5.3. This time the slope is exactly equal to two as it is expected for a coherent emission.

The estimation of the systematic uncertainty via $A_{\mathrm{CoREAS}}/A_{\mathrm{ZHAireS}}$ yields 2.9 % for S_{RD}. The statistical scatter is given by figure 5.4 as 7 %.

The two correction sets are combined to a single one and summarized in table 5.2. For the exponential n scaling the combined q_2 value is not inside of the uncertainties of the individual ones and the combined q_0 slightly outside of the ZHAireS uncertainty.

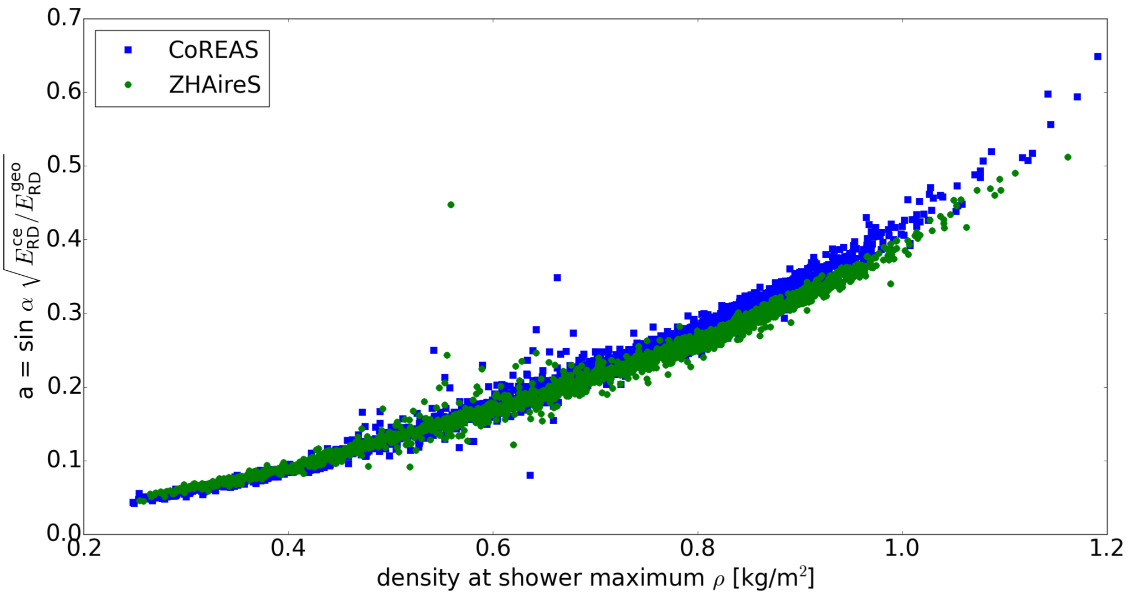

Figure 5.1: Direct comparison of the charge excess fraction for CoREAS and ZHAireS simulations depending on the atmospheric density at the shower maximum.

Table 5.1: Best fit parameters of equation (4.4) and (4.5) for CoREAS and ZHAireS using 1000 proton and 1000 iron induced random showers.

	CoREAS	ZHAireS
A	1.662 ± 0.004	1.615 ± 0.004
B	2.000 ± 0.001	2.001 ± 0.001
p_0	0.293 ± 0.007	0.291 ± 0.007
p_1	-2.78 ± 0.05	-2.74 ± 0.06

Fitting the power law with the combined corrections yields a systematic uncertainty of 3.4 %. Details of the fit are given in table 5.3. The scatter increased slightly to 7 % as shown in figure 5.5. For a direct comparison both data are plotted into the same figure which is shown in figure 5.6. It shows a good agreement between the two sets of simulations.

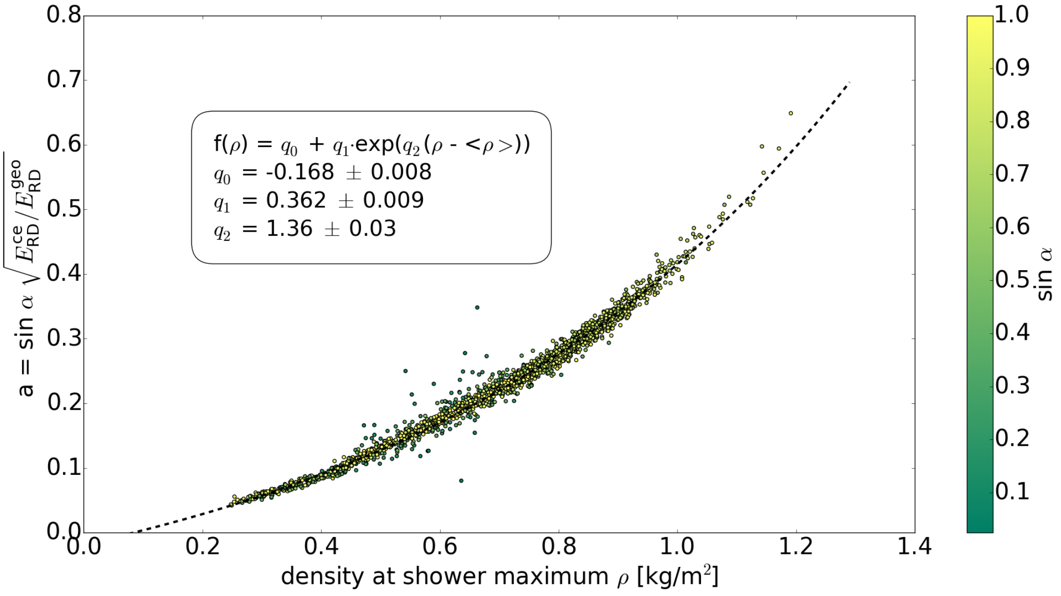

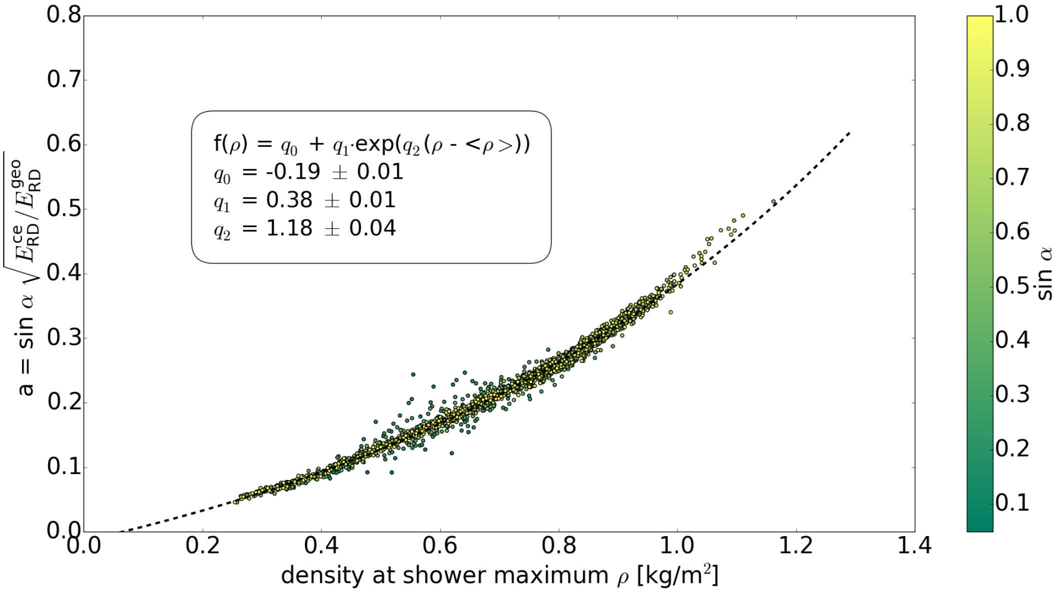

Figure 5.2: Charge excess fraction a of an air shower depending on the atmospheric density at the shower maximum for CoREAS (top) and ZHAireS (bottom).

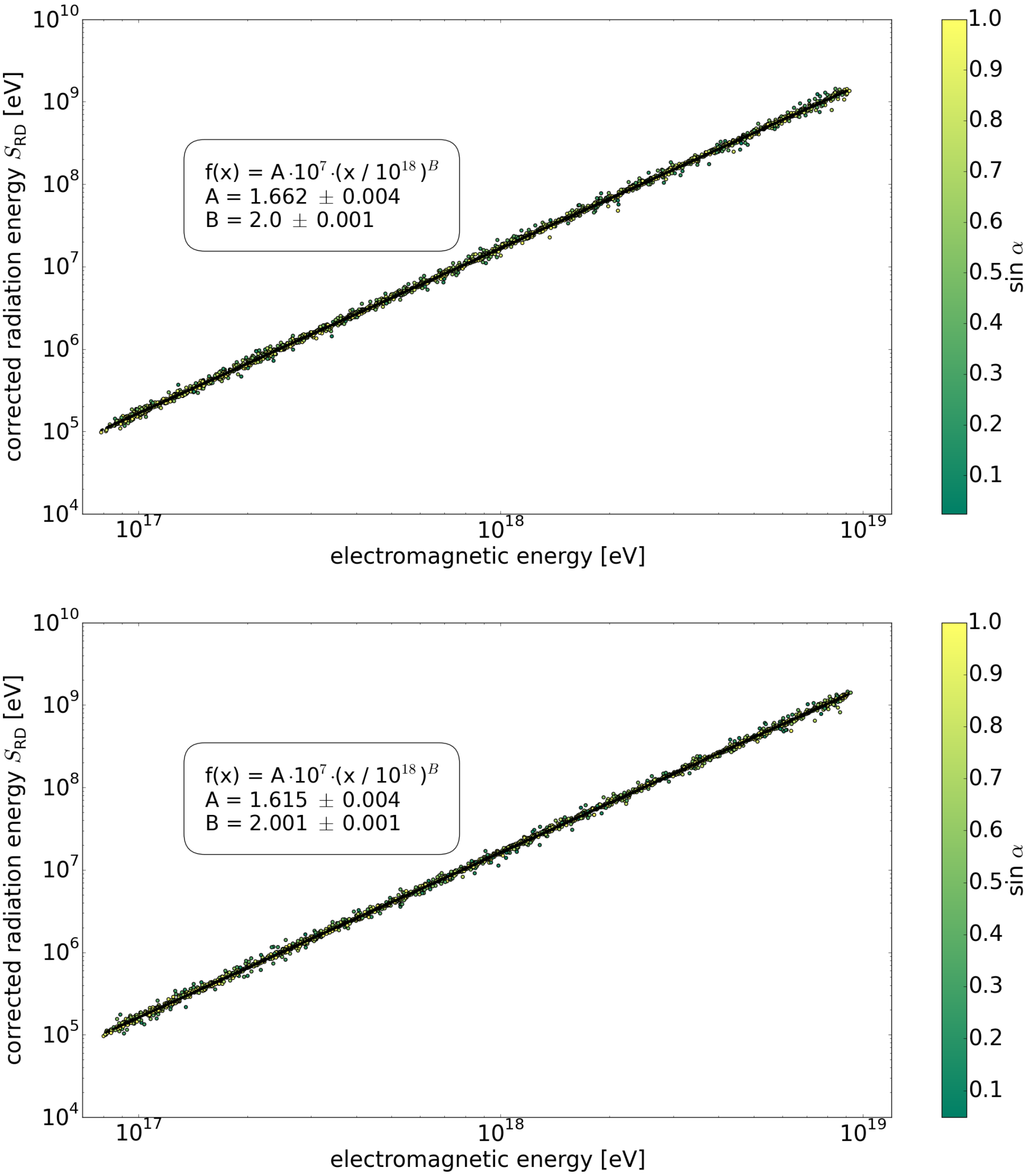

Figure 5.3: Correlation between the corrected radiation energy and the electromagnetic component of an air shower for CoREAS (top) and ZHAireS (bottom).

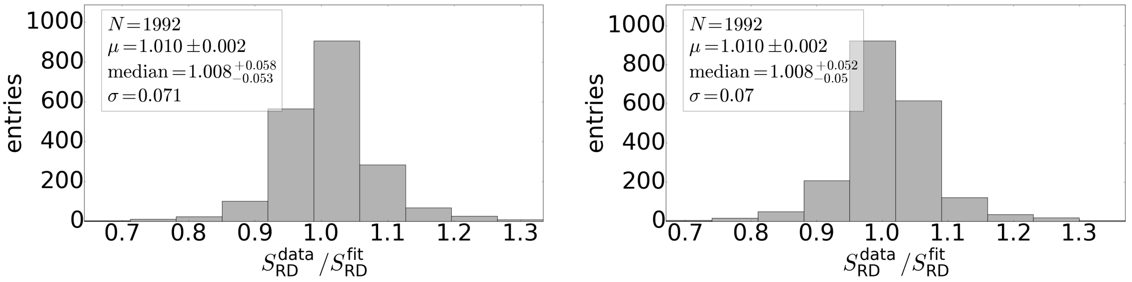

Figure 5.4: Scatter of the corrected radiation data and the fitted power law for CoREAS (left) and ZHAireS (right).

Table 5.2: Individual and combined parameters for the corrections of the radiation energy. The q_i values belong to the charge excess fraction, p_i are used in the second correction term.

	CoREAS	ZHAireS	combined
q_0	-0.168 ± 0.008	-0.19 ± 0.01	-0.176
q_1	0.362 ± 0.009	0.38 ± 0.01	0.37
q_2	1.36 ± 0.03	1.18 ± 0.04	1.29
p_0	0.293 ± 0.007	0.291 ± 0.007	0.292
p_1	-2.78 ± 0.05	-2.74 ± 0.06	-2.76

Table 5.3: Best fit parameters of equation (4.4) and (4.5) for CoREAS and ZHAireS with the combined corrections using 1000 proton and 1000 iron induced random showers.

	CoREAS	ZHAireS
A	1.663 ± 0.001	1.609 ± 0.001
B	2.0002 ± 0.0005	2.0006 ± 0.0005

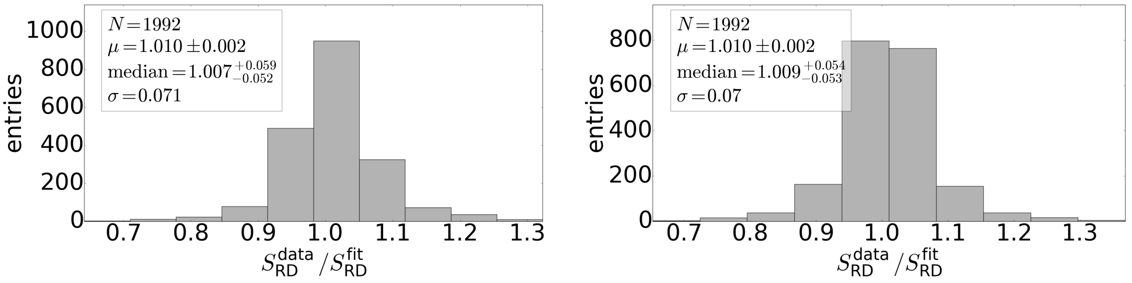

Figure 5.5: Scatter of the corrected radiation data using the combined corrections and the fitted power law for CoREAS (left) and ZHAireS (right).

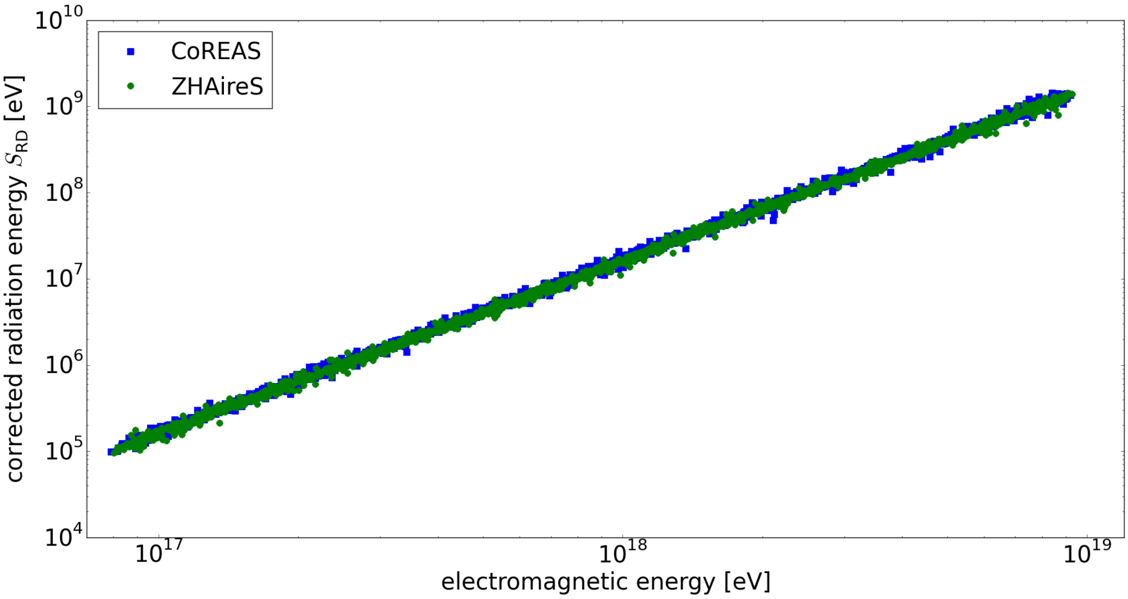

Figure 5.6: Direct comparison of the corrected radiation energy using the combined corrections for CoREAS and ZHAireS.

5.3 Detailed View at 1 EeV Showers

As in the previous chapter 1 EeV showers induced by a proton primary are compared in more details. The azimuth angle is chosen again in 30° steps from 0° to 360°. Theta is chosen in 10° steps from 10° to 70°. Data with 80° zenith angle cannot be used here anymore because CoREAS switches the computation of n internally for showers which are more horizontal than 75° to a piecewise integration. This would be inconsistent with the other datapoints and with ZHAireS and is therefore excluded.

The data is shown in figure 5.7. On average CoREAS produces approximately 4 % more radiation than ZHAireS. This is consistent with the results found in the last section. Notably the theta dependence found in the case of a constant refractive index cannot be found here.

Applying the individual corrections yields figure 5.8. The ratio gets smaller for all showers, but a small theta dependency is visible. This time the ratio decreases for more horizontal showers. But the effect is small and still compatible within the uncertainties.

Using the combined parameters for the corrections removes this dependency again. The data is shown in figure 5.9. On average the difference between CoREAS and ZHAireS is around 3 % which is in a good agreement with the results from the power law fit without a clear correlation to the zenith angle.

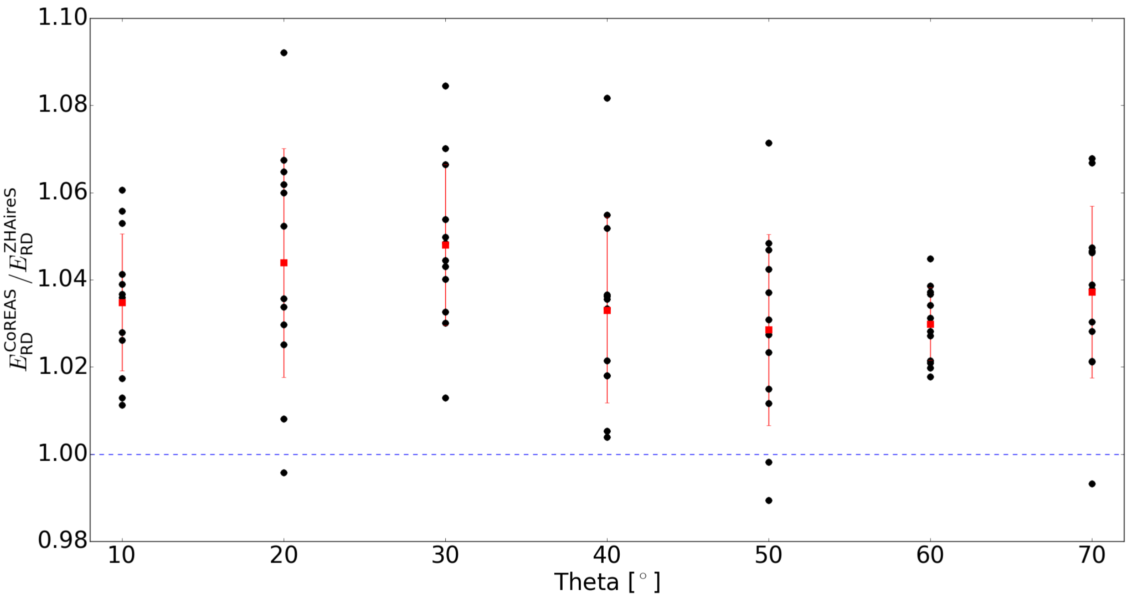

Figure 5.7: Ratio of the radiation energy of CoREAS and ZHAireS for different azimuth angles plotted against the zenith angle. In red the mean value and the standard deviation is shown.

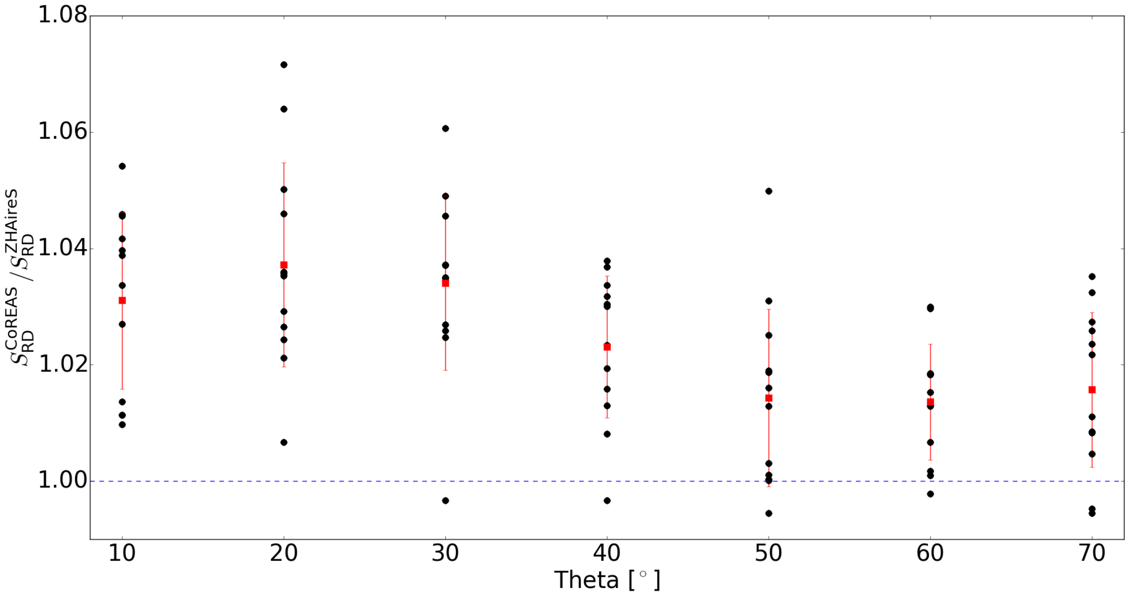

Figure 5.8: Ratio of the corrected radiation energy using the individual corrections of CoREAS and ZHAireS for different azimuth angles plotted against the zenith angle. In red the mean value and the standard deviation is shown.

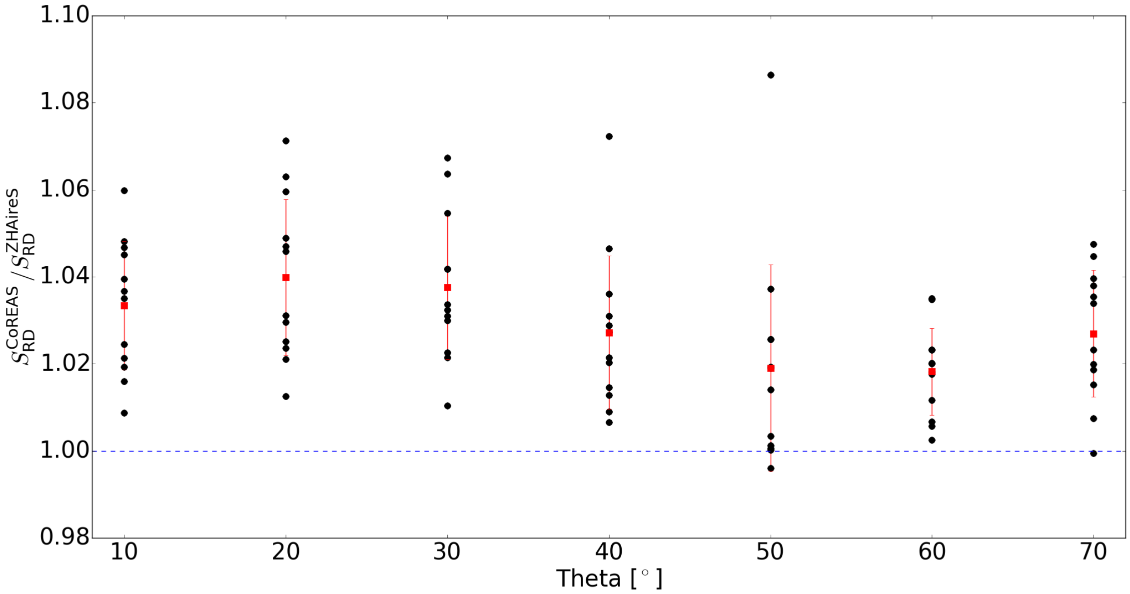

Figure 5.9: Ratio of the corrected radiation energy using the combined corrections of CoREAS and ZHAireS for different azimuth angles plotted against the zenith angle. In red the mean value and the standard deviation is shown.

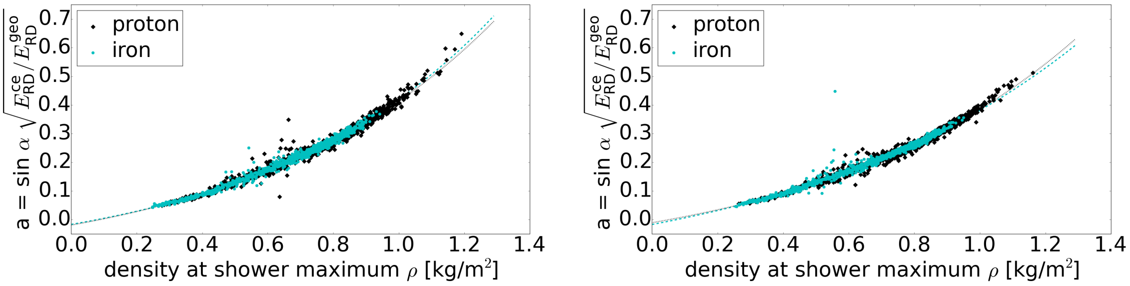

Figure 5.10: Difference in the charge excess fraction between proton and iron primaries for CoREAS (left) and ZHAireS (right).

5.4 Difference Proton and Iron Primary

The proton and iron showers are now analyzed independently to check the influence of the primary particle type for the radiation energy. Proton are used as they are very common and lightweight whereas iron primaries are the heaviest among all expected primaries. Therefore this can be used as a benchmark to test if this method allows to separate different primaries and contribute in the composition studies.

Looking at the charge excess fraction shown in figure 5.10 one can see a good agreement between the proton and iron data for CoREAS and ZHAireS. This impression is also reinforced by taking a look at the fit data in table 5.4. For CoREAS none of the difference is significant with the given fit uncertainties. For ZHAireS all parameters

Table 5.4: Best fit parameters for the charge excess fraction (equation (4.2)) with CoREAS and ZHAireS for proton and iron primaries. The dataset contains 1000 proton and 1000 iron induced random showers.

	q_0	q_1	q_2
CoREAS Proton	-0.17 ± 0.01	0.37 ± 0.01	1.34 ± 0.04
CoREAS Iron	-0.158 ± 0.008	0.352 ± 0.008	1.41 ± 0.04
ZHAireS Proton	-0.168 ± 0.009	0.36 ± 0.01	1.26 ± 0.03
ZHAireS Iron	-0.21 ± 0.01	0.40 ± 0.01	1.11 ± 0.04

Table 5.5: Best fit parameters for the corrected radiation energy (equation (4.4) and (4.5)) with CoREAS and ZHAireS for proton and iron primaries. The dataset contains 1000 proton and 1000 iron induced random showers.

	A	B	p_0	p_1
CoREAS Proton	1.697 ± 0.006	1.993 ± 0.002	0.34 ± 0.01	-2.46 ± 0.09
CoREAS Iron	1.633 ± 0.004	2.007 ± 0.001	0.246 ± 0.008	-3.17 ± 0.08
ZHAireS Proton	1.653 ± 0.006	1.994 ± 0.002	0.33 ± 0.01	-2.47 ± 0.09
ZHAireS Iron	1.583 ± 0.004	2.006 ± 0.001	0.232 ± 0.008	-3.23 ± 0.09

have changed significantly but this has only a minor influence on the fit. One can see that the iron data has lower densities at X_{max} compared to the proton data. Due to the higher mass of iron the shower develops earlier in the atmosphere and therefore reaches its maximum at higher altitudes with a lower density. At higher densities one can see that the order of the fits changed from CoREAS to ZHAireS. CoREAS predicts a slightly larger charge excess fraction for an iron primaries than for a proton. In ZHAireS this is the other way round.

The individual scalings of the charge excess fraction is used for the fits of S_{RD}. The results are summarized in table 5.5. Again each value differs significantly, however in the final power law plot in figure 5.11 this differences are not visible.

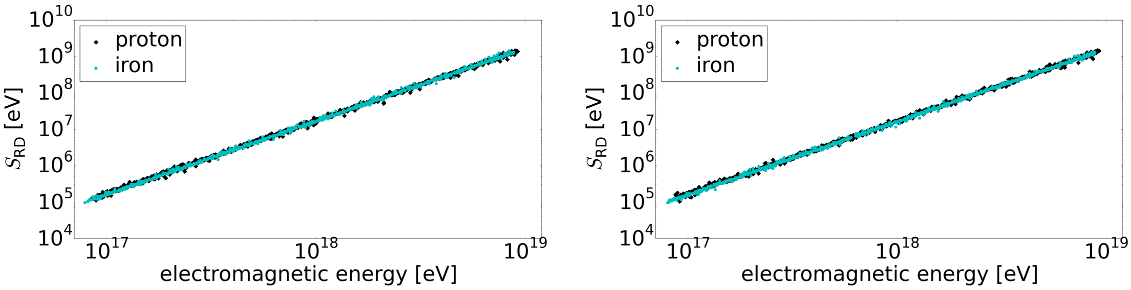

Figure 5.11: Difference of the corrected radiation energy between proton and iron primaries for CoREAS (top) and ZHAireS (bottom).

Table 5.6: Corrected radiation energy for different values of the refractive index at sea level. For ZHAireS a 1 EeV proton primary is used, in CoREAS the primary particle is an iron with the same energy. In both cases the geometry is fixed to a zenith angle of 50° coming from south. Each cell shows the mean of 20 (CoREAS) or 40 (ZHAireS) simulations which differ only in the initial seed. The quoted uncertainty is the uncertainty of the mean.

n - 1	CoREAS	ZHAireS
2.04×10^{-4} ($-30\,\%$)	(10.64 ± 0.04) MeV ($-10.4\,\%$)	(12.46 ± 0.05) MeV ($-10.4\,\%$)
2.34×10^{-4} ($-20\,\%$)	(11.04 ± 0.04) MeV ($-7.0\,\%$)	(12.93 ± 0.05) MeV ($-7.0\,\%$)
2.63×10^{-4} ($-10\,\%$)	(11.47 ± 0.04) MeV ($-3.4\,\%$)	(13.33 ± 0.06) MeV ($-4.1\,\%$)
2.77×10^{-4} ($-5\,\%$)	(11.58 ± 0.05) MeV ($-2.4\,\%$)	(13.43 ± 0.07) MeV ($-3.4\,\%$)
2.92×10^{-4}	(11.87 ± 0.04) MeV	(13.90 ± 0.06) MeV
3.07×10^{-4} ($+5\,\%$)	(12.05 ± 0.05) MeV ($+1.5\,\%$)	(13.93 ± 0.06) MeV ($+0.2\,\%$)
3.21×10^{-4} ($+10\,\%$)	(12.19 ± 0.04) MeV ($+2.7\,\%$)	(14.29 ± 0.05) MeV ($+2.8\,\%$)
3.50×10^{-4} ($+20\,\%$)	(12.55 ± 0.05) MeV ($+5.7\,\%$)	(14.66 ± 0.07) MeV ($+5.5\,\%$)
3.80×10^{-4} ($+30\,\%$)	(12.81 ± 0.04) MeV ($+7.9\,\%$)	(14.96 ± 0.06) MeV ($+7.6\,\%$)

Comparing only the iron or proton data of CoREAS and ZHAireS the fit results are very close. Its interesting that both simulations yields an exponent B slightly lower than 2 for a proton primary and slightly higher than 2 for an iron primary. Comparing the A values again one can see that a proton induced air shower has a 4 % higher corrected radiation energy than an iron induced air showers.

The fraction of the primary energy that enters the electromagnetic component of the air shower is different for proton and iron primaries. Hence, in a correlation with the primary energy different radiation energies would be expected as the radiation is mostly emitted by the electromagnetic shower component. But in the analysis the radiation energy is correlated with the electromagnetic energy directly. Thus, there should be no difference between proton and iron induced air showers. Since the density at X_{max} is used in the corrections this effect cannot be due to the different average X_{max} of proton and iron induced air showers. It is hence unclear what causes this differences.

5.5 Scaling with the Refractive Index

Just by comparing the results of the previous chapter with the current one it is clear that the refractive index has a strong influence on the emitted radiation energy. This dependency is now studied in detail for the exponential n scaling. The refractive index at sea level is changed and the resulting radiation energies are compared. Using data from the Global Data Assimilation System (GDAS) the yearly fluctuations of the air refractivity at the Pierre Auger Observatory is 7 % [12].

For the simulations iron primaries are used for CoREAS. Due to the higher mass the scatter of the X_{max} values is lower for iron. Therefore, the uncertainties of S_{RD} is smaller for the same number of simulations. For ZHAireS the air showers are induced by a proton primary. To get the same accuracy the number of simulations is increased from 20 to 40. The resulting S_{RD} values for the different refractivities $n-1$ are shown in table 5.6.

The difference between proton and iron primaries can therefore be studied once again for 1 EeV showers with the usual geometry. For this setup the difference is around 16 % which is far above the estimated 4 % of the previous section and inconsistent with the power law fit for the CoREAS simulations. It must therefore depend on either the energy or the shower direction.

Comparing the relative change one can see that the scaling of S_{RD} agrees very well for both programs. A change of $+10\,\%$ ($-10\,\%$) yields around 3 % more (4 % less) radiation energy energy. For the relevant fluctuations this is again small compared to the experimental uncertainty.

5.6 Scaling with the Geomagnetic Field

The contribution of the geomagnetic emission depends on the magnetic field. This dependency was ignored until now because all simulations were using the same magnetic field of the AERA site. Now the magnetic field strength is varied for a fixed inclination of $-35.7°$. The magnetic field strength of AERA $B_{\mathrm{Auger}} = 0.243\,\mathrm{G}$ is used as a reference for the analysis. 100 proton induced air showers with a fixed geometry of 50° zenith angle coming from south are simulated with an magnet field strength uniformly distributed in $1 \cdot B_{\mathrm{Auger}}$ to $3 \cdot B_{\mathrm{Auger}}$. This covers all of the relevant magnetic field strengths on earth.

The correction of the geomagnetic part is extended by $(B/B_{\mathrm{Auger}})^k$ and the charge excess fraction consequently by $(B/B_{\mathrm{Auger}})^{-k/2}$. The parameter k is determined to 1.74 ± 0.02 for CoREAS and 1.75 ± 0.02 for ZHAireS via a fit to the data. On a naive approach one would expect k to be 2 as the amplitude of the electric field scales proportional with the magnitude of the Lorentz force which is proportional to the magnitude of the geomagnetic field. But due to scattering in the shower front the average drift velocity in the direction of the Lorentz force is smaller than the velocity of the particles in the shower front which explains the difference in k [12].

Adding this corrections yields figure 5.12. The data shows a big scattering per shower, however a small second order effect is visible. To enlarge this dependency the plot is repeated with an magnetic field strength up to $7 \cdot B_{\mathrm{Auger}}$ and shown in figure 5.13. The second order dependency is now clearly visible, however it seems like the necessary correction to incorporate this effect depends additionally on the zenith angle and the $\sin(\alpha)$ value. For the shown data a scaling with $(a \cdot \tanh(b \cdot B))^2$ would take the second order effect into account, a generalization for all zenith and geomagnetic angles seems to be hard to find [19]. But the influence for the relevant magnetic fields on earth is small thus this effect can be neglected.

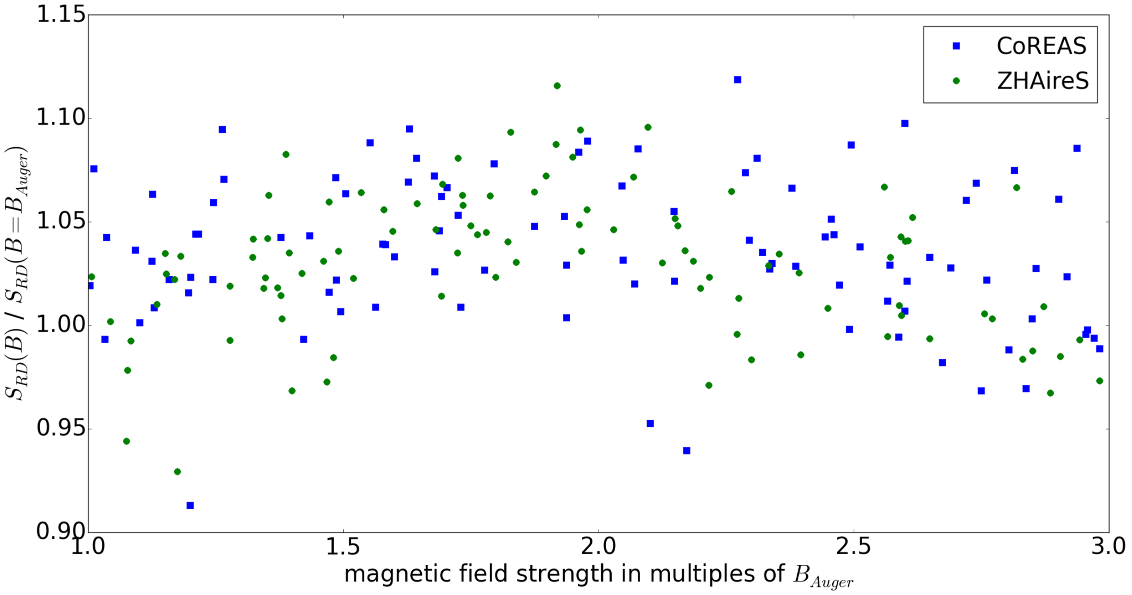

Figure 5.12: Corrected radiation energy including first magnetic field correction depending on the magnetic field strength. The showers are induced by an iron primary with 1 EeV primary energy, an zenith angle of 50° and coming from south. The magnetic field strength is expressed as multiple of the magnet field at the Pierre Auger Observatory $B_{\mathrm{Auger}} = 0.243\,\mathrm{G}$, the direction corresponds to the one at the Pierre Auger Observatory.

This yields the final formula for the corrected radiation energy for all magnetic fields on Earth.

$$S_{\mathrm{RD}} = \frac{E_{RD}}{a'(\rho)^2 + (1 - a'(\rho)^2)\sin^2\alpha (B/B_{\mathrm{Auger}})^{1.745}} \frac{1}{(1 - p_0 + p_0 \exp\left[p_1(\rho - \langle\rho\rangle)\right])^2} \tag{5.1}$$

with

$$a'(\rho) = a(\rho)/(B/B_{\mathrm{Auger}})^{0.8725}. \tag{5.2}$$

5.7 Assumption of Radial Symmetry

In the derivation of the method a radial symmetry for the LDFs of geomagnetic emission and charge excess was assumed. Thus there should be no difference in the radiation energy between the positive and negative $\vec{v} \times (\vec{v} \times \vec{B})$ arm where the two components decouple to the x- and y-polarization. To verify this, 40 showers with an 1 EeV proton primary are simulated with antennas on both axes. The shower geometry is fixed as usual to 50° zenith angle coming from south.

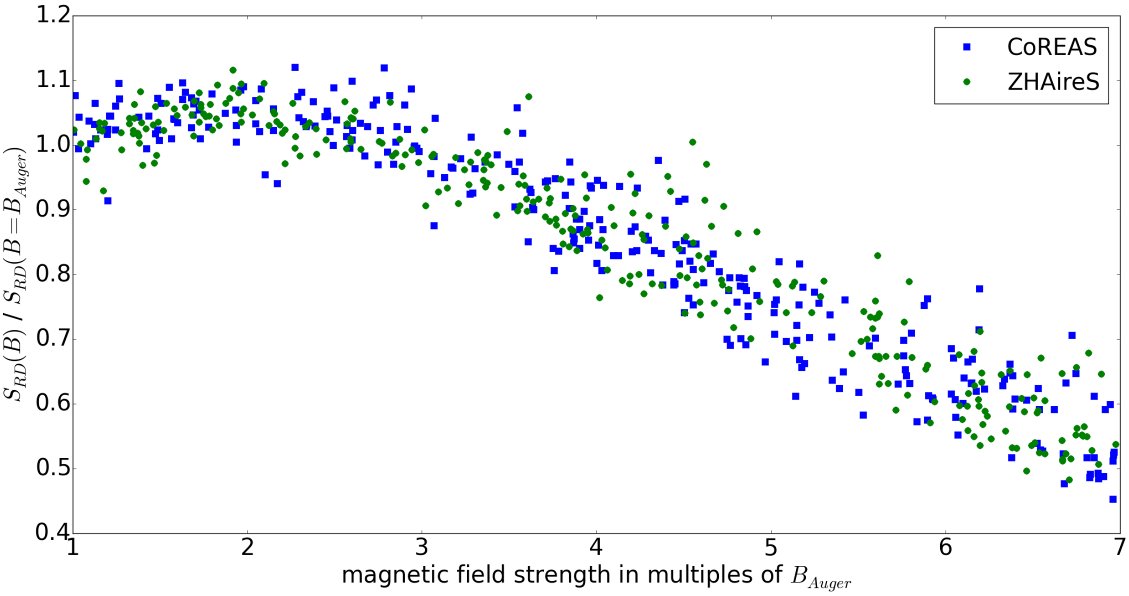

Figure 5.13: Corrected radiation energy including first magnetic field correction depending on the magnetic field strength. The showers are induced by an iron primary with 1 EeV primary energy, an zenith angle of 50° and coming from south. The magnetic field strength is expressed as multiple of the magnet field at the Pierre Auger Observatory $B_{\text{Auger}} = 0.243\,\text{G}$, the direction corresponds to the one at the Pierre Auger Observatory.

Table 5.7: Radiation energy for CoREAS and ZHAireS with antenna only on positive or negative $\vec{v} \times (\vec{v} \times \vec{B})$ axis. 40 Showers induced by a proton primary with zenith angle of 50° coming from south are simulated, the quoted uncertainty is the uncertainty of the mean.

	COREAS	ZHAireS
pos. $\vec{v} \times (\vec{v} \times \vec{B})$ axis	$(13.7 \pm 0.1)\,\text{MeV}$	$(13.3 \pm 0.2)\,\text{MeV}$
neg. $\vec{v} \times (\vec{v} \times \vec{B})$ axis	$(13.3 \pm 0.2)\,\text{MeV}$	$(12.8 \pm 0.1)\,\text{MeV}$

Figure 5.14 shows the mean LDF for CoREAS and ZHAireS for both axes. Events with an $X_{\text{max}} > 800\,\text{g}\,\text{cm}^{-2}$ are ignored for the calculation of the mean LDF because the form of the LDF depends on the X_{max} value and changes for higher shower maxima. The resulting E_{RD} values are presented in table 5.7.

Although the difference of the LDFs are small the results are significantly different. This can be explained by the differences heights above ground of the antennas on the two axes. Therefore, the shower sees a different effective refractive index which has an influence on the emitted radio signal.

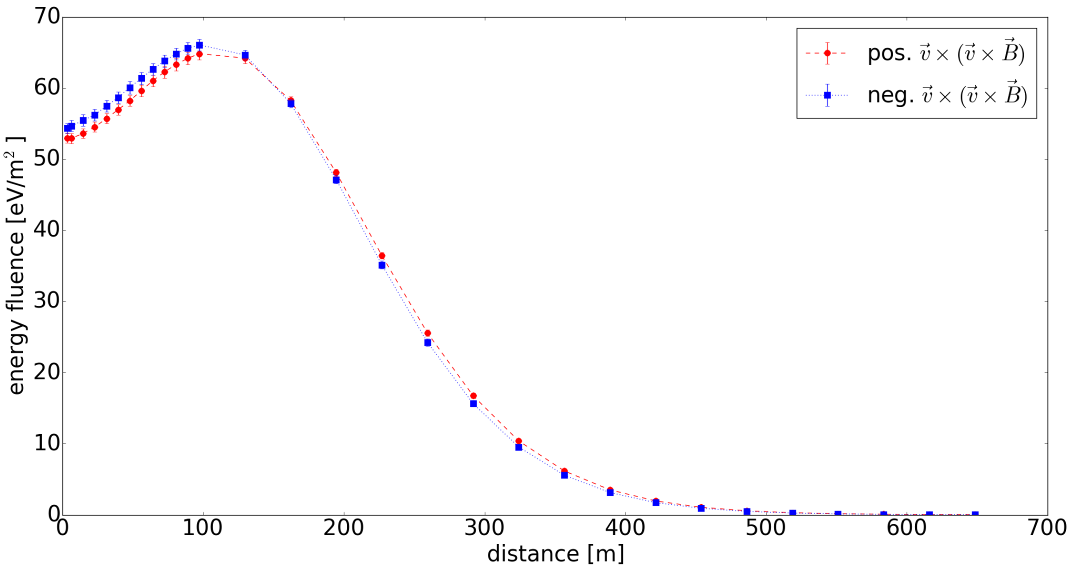

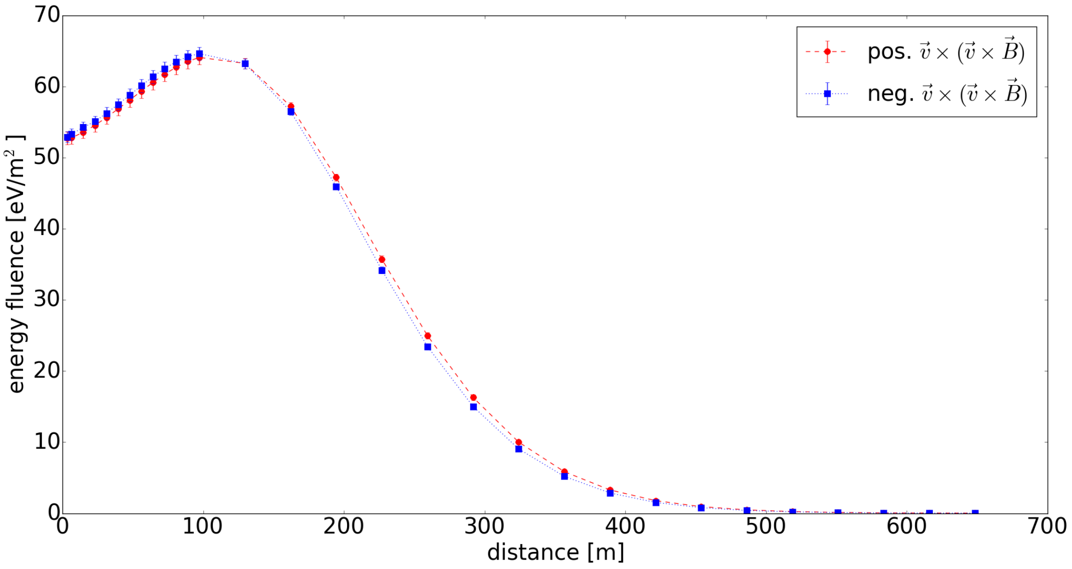

Figure 5.14: Mean LDF for COREAS (top) and ZHAireS (bottom) after the $X_{\max}$ cut. The air showers are induced by an 1 EeV proton primary with an zenith angle of 50° coming from south. The quoted uncertainty at each data point is the uncertainty of the mean.

5.8 Corrections without the Shower Maximum

For real measurements $X_{\max}$ is typically unknown or has large experimental uncertainties. Hence it is necessary to have another set of correction parameter that does not rely on knowing $X_{\max}$. The analysis is repeated assuming the average $\langle X_{\max} \rangle = 669\,\mathrm{g\,cm^{-2}}$ and correcting for the zenith angle only.

Table 5.8: Individual and combined parameters for the corrections of the radiation energy without knowing X_{max}. The q_i values belong to the charge excess fraction, p_i are used in the second correction term.

	CoREAS	ZHAireS	combined
q_0	-0.24 ± 0.02	-0.19 ± 0.01	-0.21
q_1	0.44 ± 0.02	0.38 ± 0.01	0.392
q_2	1.12 ± 0.04	1.22 ± 0.05	1.16
p_0	0.220 ± 0.009	0.238 ± 0.009	0.224
p_1	-3.3 ± 0.1	-3.2 ± 0.1	-3.325

Table 5.9: Best fit parameters for CoREAS and ZHAireS using the combined corrections without knowing X_{max}. The dataset contains 1000 proton and 1000 iron induced random showers.

	CoREAS	ZHAireS
A	1.647 ± 0.001	1.593 ± 0.001
B	1.9984 ± 0.0005	1.9977 ± 0.0005

The results for the charge excess ratio and S_{RD} are directly combined into a single set of parameters and are given in table 5.8. They are used to fit the power law again, the results are shown by table 5.9.

A possible explanation for the slope being slightly but significantly smaller than 2 was found in [12]. The average X_{max} increases linearly width the logarithm of the primary energy, i.e. a shower with a higher primary energy develops deeper into the atmosphere. Due to the higher atmospheric density more radiation energy should be emitted. This effect cannot be compensated without knowing X_{max}. Thus, the radiation energy is slightly underestimated for higher energies which results in $B < 2$. The systematic uncertainty is still 3.4 %, but the scatter has increased to 7.6 % (7.5 %) for CoREAS (ZHAireS) as shown in figure 5.15.

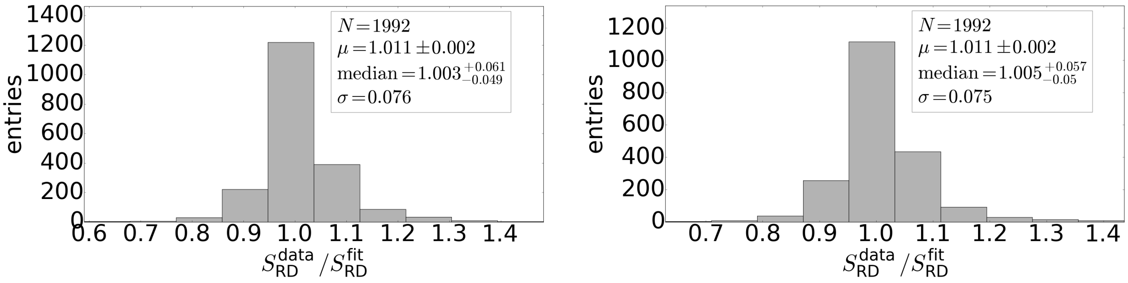

Figure 5.15: Scatter of the corrected radiation data using the combined corrections without knowing X_{max} of the fitted power law for CoREAS (left) and ZHAireS (right).

6 Fitting the Lateral Distribution Function to measured Data

The asymmetric profile due to the superposition of the two radio emission mechanisms (cf. section 1.2) radio LDF can be described by the sum of two gaussian functions. Due to correlations of different parameters the number of free parameters can be decreased. This is especially helpful if only a small number of antenna triggered in an experiment. The LDF is fitted and free parameters are replaced by constants in the following.

6.1 Reducing the Number of free Parameters

Due to the two radio emission processes the LDF can be described as the sum of two gaussian functions in two dimensions [20]. The general parameterization is given in equation 6.1, where the x,y coordinates are used for the $\vec{v} \times \vec{B}$, $\vec{v} \times (\vec{v} \times \vec{B})$ axes respectively. The radial symmetry is enforced for each gaussian, however the total LDF is asymmetric.

$$f(x, y) = A_+ \exp\left(-\frac{(x - X_+)^2 + (y - Y_+)^2}{\sigma_+^2}\right) - A_- \exp\left(-\frac{(x - X_-)^2 + (y - Y_-)^2}{\sigma_-^2}\right) \tag{6.1}$$

In AERA the number of triggered station data can be too small for a good fit with eight free parameters. Therefore, an alternative formulation is used that already contains some results from simulation studies [21].

$$f(\vec{r}) = A\left(\exp\left(-\frac{\vec{r} + C_1\vec{e}_{\vec{v}\times\vec{B}} - \vec{r}_{\text{core}}}{\sigma^2}\right) - C_0 \exp\left(-\frac{\vec{r} + C_2\vec{e}_{\vec{v}\times\vec{B}} - \vec{r}_{\text{core}}}{(C_3 \exp(C_4 \cdot \sigma))^2}\right)\right), \tag{6.2}$$

where $\vec{r}$ denotes the station position and $\vec{r}_{\text{core}}$ the position of the core in the shower plane.

An optional shift in $\vec{v} \times (\vec{v} \times \vec{B})$ directions was shown to be unnecessary for a good fit as it is much smaller than the current precision [20]. Also a correlation of σ_+ and σ_- can be found which allows to remove one more parameter. The constants C_0 to C_4 can be estimated with simulations. This reduces the number of free parameters to the amplitude, A, the width, σ, and the shower core, $\vec{r}_{\text{core}}$.

An example of a successful fit is shown in figure 6.1. For the LDF-fits the simulations are performed with antennas in the full two dimensional shower plane distributed on a star shape pattern. The simulations of section 2.3 can thus be reused here. While the data is interpolated for the visualization, the fit takes only the simulated antenna positions into account. The black lines show the contour lines of the fitted LDF.

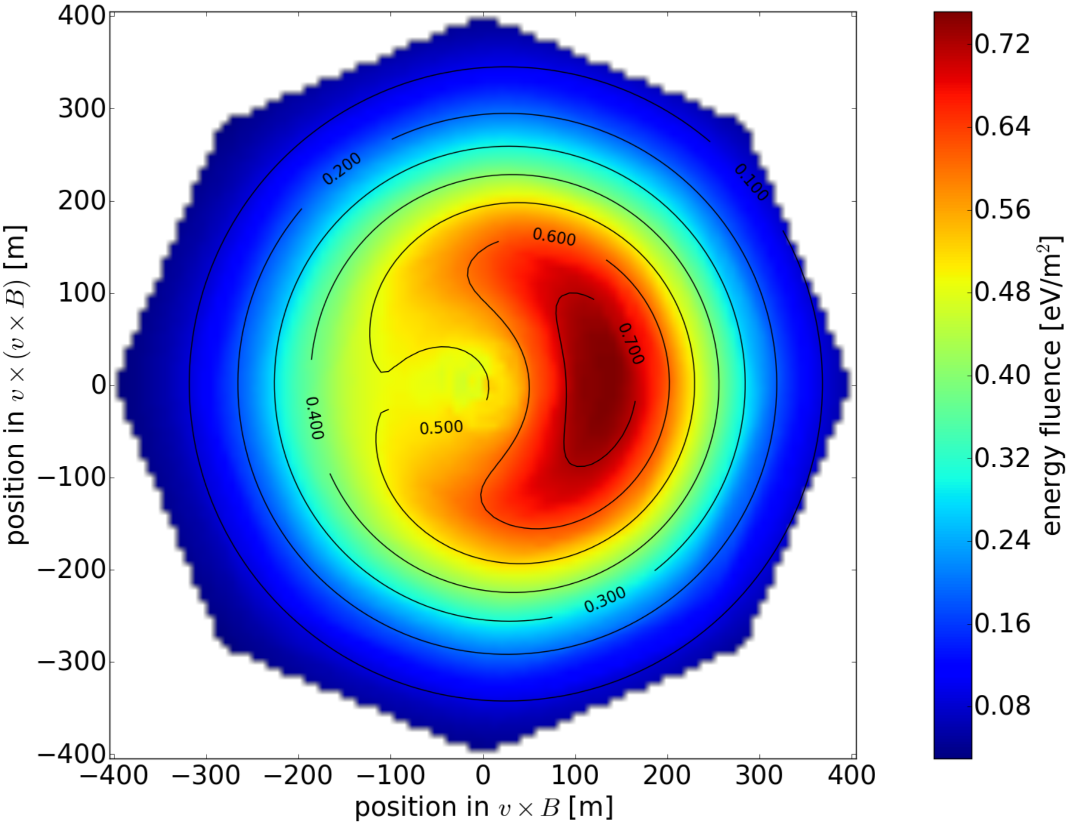

Figure 6.1: Visualization of the LDF in the shower plane for an air shower with a 1 EeV proton primary, a zenith angle of 50° and coming from south. The horizontal,vertical and diagonal values are actual data, the rest is interpolated. The black lines are the contour lines of the fitted LDF.

Unfortunately this parameterization depends on a specific detector environment as magnetic field, refractive index and height above sea level. As the data of section 2.3 is reused here the magnetic field of the AERA detector and the exponential n is used but the observer level is placed at sea level. This results in values for the constants C_i which are different from [21]. The propagation of the radio signal increases the spread of the gaussians and their position in the shower plane. However, the reference values are added in the following plots for a comparison.

6.2 Estimation of the LDF Constants

At first the full LDF is fitted to the data. The fit is constraint by demanding $A_{-} > 10^{-10}$ and $|x_{-}|$ less than half of the total footprint size. Without this constraints the negative gaussian is sometimes placed far away from the shower core with amplitudes less than 10^{-30}. No correlation of these fits with the shower geometry could be found.

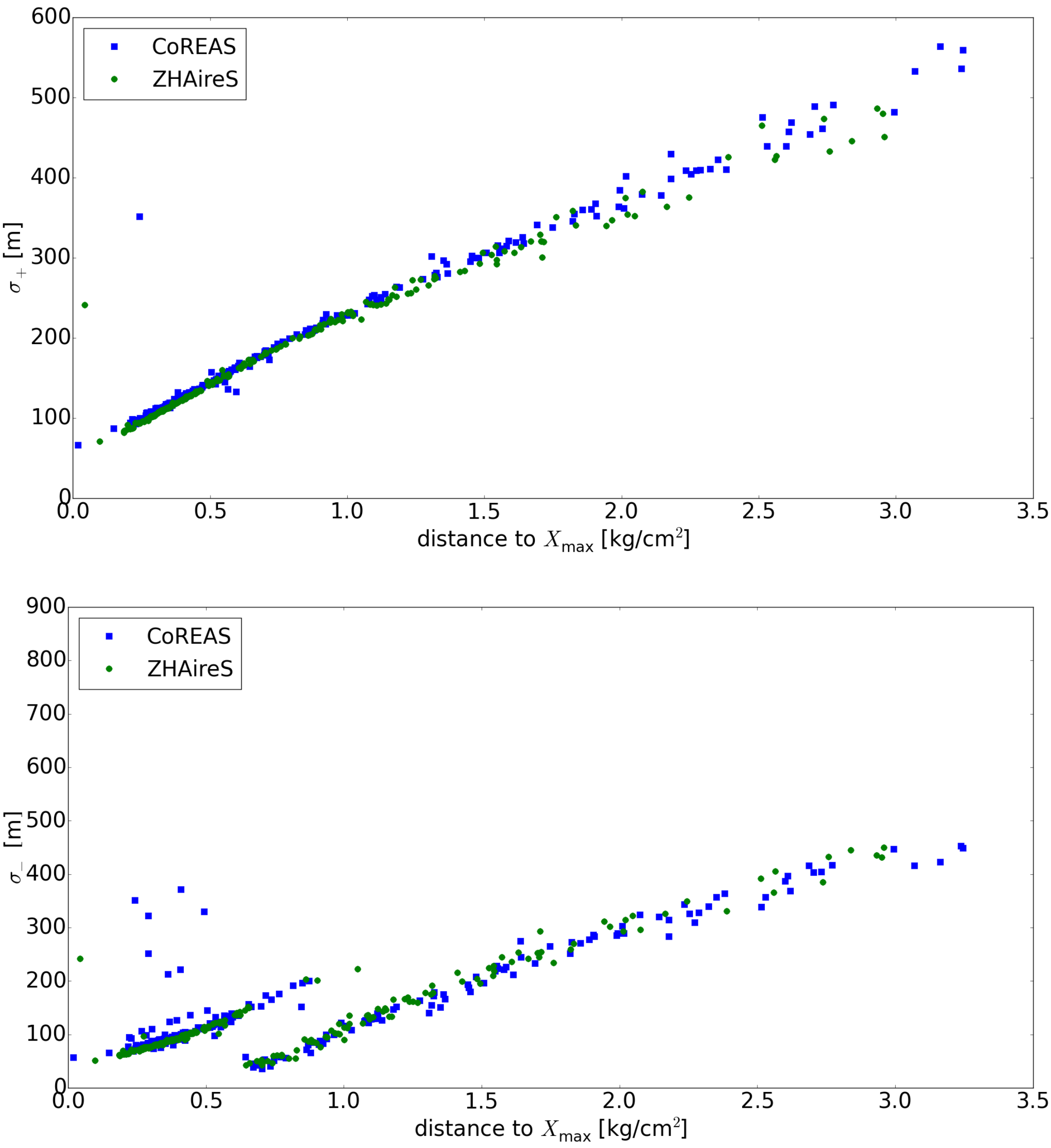

Figure 6.2: Fit results of the width of the two gaussians peaks as a function of the distance to the shower maximum. The upper plots shows the positive gaussian, the lower one the negative.

Figure 6.2 shows the dependency of the fit results for $\sigma_\pm$ on the distance to the shower maximum. This is a direct consequence of the propagation of the radio signal. For zenith angles larger than 50° a second arm gets visible for σ_-. Therefore, only smaller zenith angles are used to studies the correlation between $\sigma_\pm$.

In figure 6.3 σ_- is plotted against σ_+. An additional $\sin(\alpha) < 0.2$ cut is used to remove outliers. For showers with a lower geomagnetic angle the geomagnetic peak

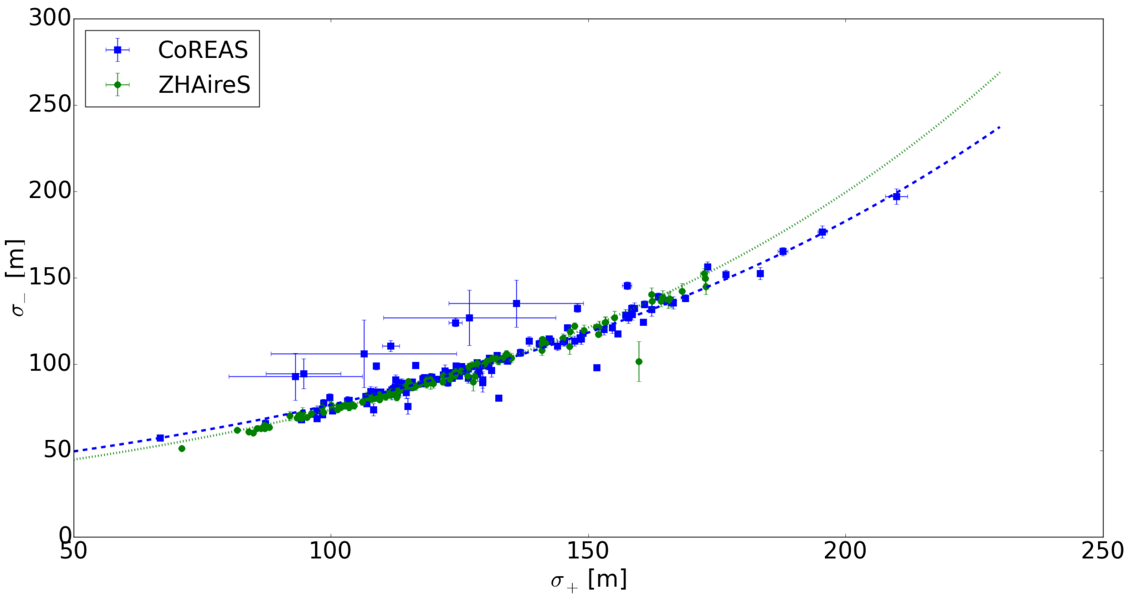

Figure 6.3: Correlation of the σ values for both gaussian peaks. Only showers with zenith angle less than 50° and a $\sin(\alpha)$ value larger than 0.2 are considered.

Table 6.1: Fit parameters of the σ dependency for CoREAS and ZHAireS simulations. The reference values are added for a comparison.

	CoREAS	ZHAireS	reference
C_3/m	32.1 ± 0.4	27.2 ± 0.3	16.25
$C_4 \cdot 10^4$m	87.0 ± 0.8	99.5 ± 0.5	79.00

gets small which makes is harder to fit them correctly. An exponential law

$$\sigma_- = C_3 \exp(C_4 \cdot \sigma_+) \tag{6.3}$$

can be fitted. The results are given in table 6.1. For the reference values the uncertainties are unknown. The difference between CoREAS and ZHAireS could be explained by small differences in the X_{max} distribution for both simulations.

Adding this correlation to equation 6.2 the remaining constants C_0 to C_2 are fitted in a combined fit. The results are shown in figure 6.4, 6.5 and 6.6.

For C_0 the fitted values are much smaller than the reference line shown in black. This is directly connected to the σ correlation. The integral of both gaussian functions can be used to calculate the charge excess fraction a. As C_3 is much bigger than the reference value this would lead to higher a values as expected. Hence, C_0 must be smaller to compensate this effect.

Figure 6.5 shows smaller values for C_1 for vertical showers than the reference value. This is caused by the additional propagation of the radio signal which increase the shift. For CoREAS the results are in agreement with a decrease of C_1 for all zenith

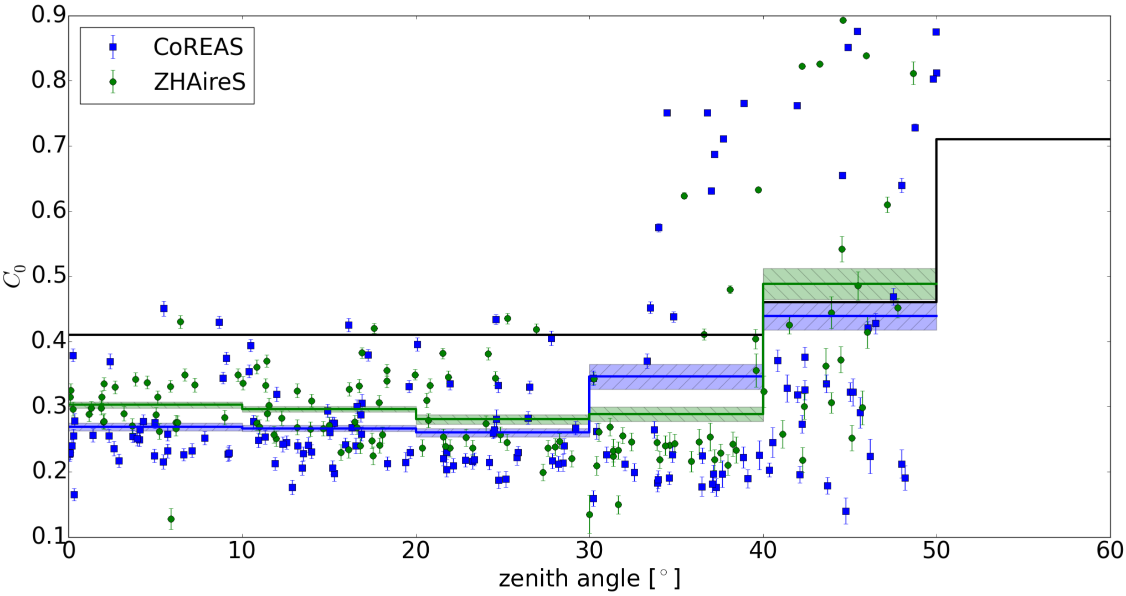

Figure 6.4: Fit results for the constant C_0 plotted against the zenith angle. The mean value and the error of the mean are shown by the solid line and the colored band for a binning in 10° steps. In black the reference value is shown.

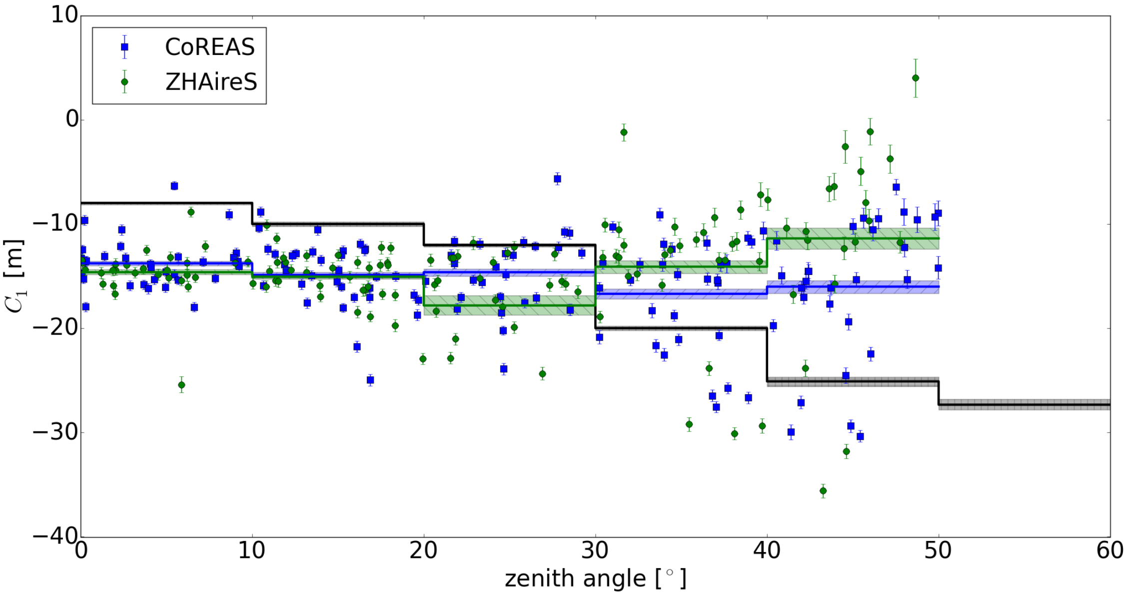

Figure 6.5: Fit results for the constant C_1 plotted against the zenith angle. The mean value and the error of the mean are shown by the solid line and the colored band for a binning in 10° steps. In black the reference value is shown.

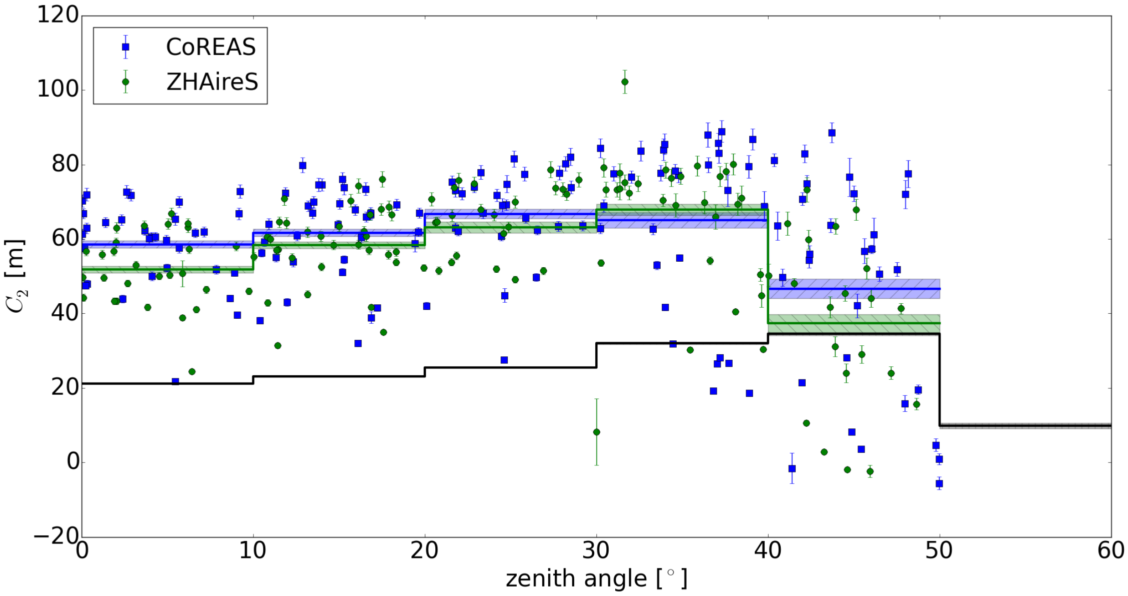

Figure 6.6: Fit results for the constant C_2 plotted against the zenith angle. The mean value and the error of the mean are for a binning in 10° steps. In black the reference value is shown.

angles but with a smaller slope than the reference line. In ZHAireS the mean value of C_1 increases with higher zenith angles. But the data shows a large scatter thus more simulations would be needed for a reliable result.

The results of C_2 shown in figure 6.6 are again bigger than the reference line due to the propagation. The CoREAS and ZHAireS values are close to each other. But the decrease of C_2 starts already at smaller zenith angles compared to the reference line.

The parameter σ depends on the distance to the shower maximum. In a first order approximation this can be described as a linear function as shown in figure 6.7. An offset and a small difference in the slope can be seen for CoREAS and ZHAireS. For the relevant distances at AERA this differences are small. Hence, σ can be used as a simple estimator for the shower maximum.

The amplitude A is correlated with the primary energy. This dependency is shown in figure 6.8, the results for CoREAS and ZHAireS agree very well. The correlation can be described as a quadratic power law. This could be used to estimate the primary energy. But combining all the results of this thesis a better approach to reconstruct the primary energy can be used.

Starting with a measurement of an radio event the LDF is fitted to the station data. An integration yields the total radiation energy E_{RD}. Correcting this energy for all the effects mentioned in the last chapter and using the found power law the electromagnetic energy of the shower can be calculated. For simplicity the mapping between electromagnetic and calorimetric energy is reduced to a constant shift of 2 % [19]. Then the primary energy can by reconstructed with the data driven method presented in [13].

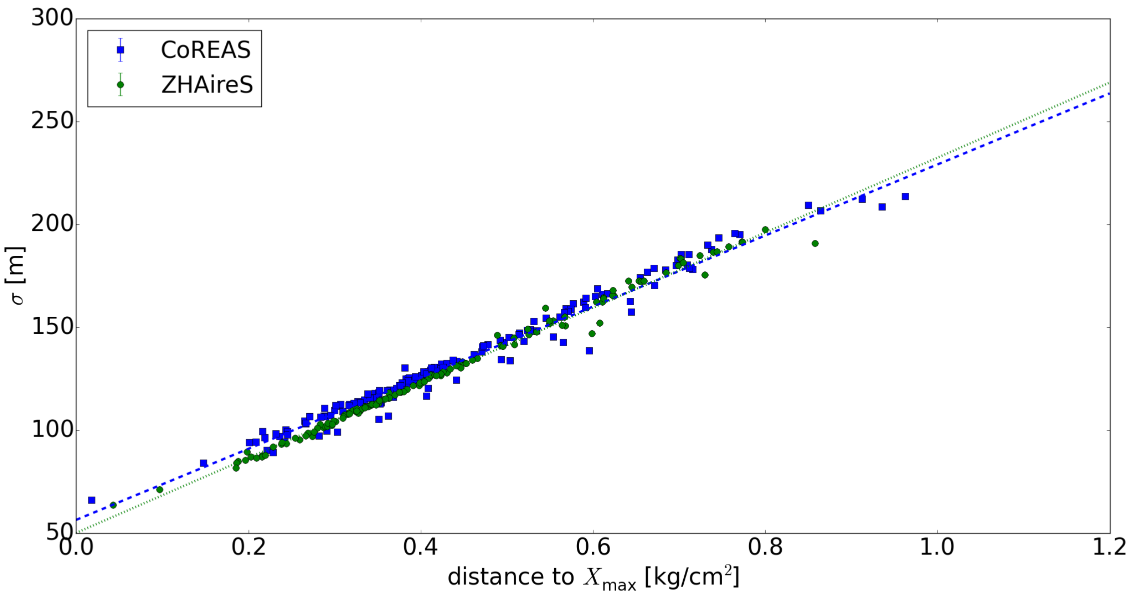

Figure 6.7: Correlation of σ on the primary energy for CoREAS and ZHAireS. A linear fit is used as a first order approximation.

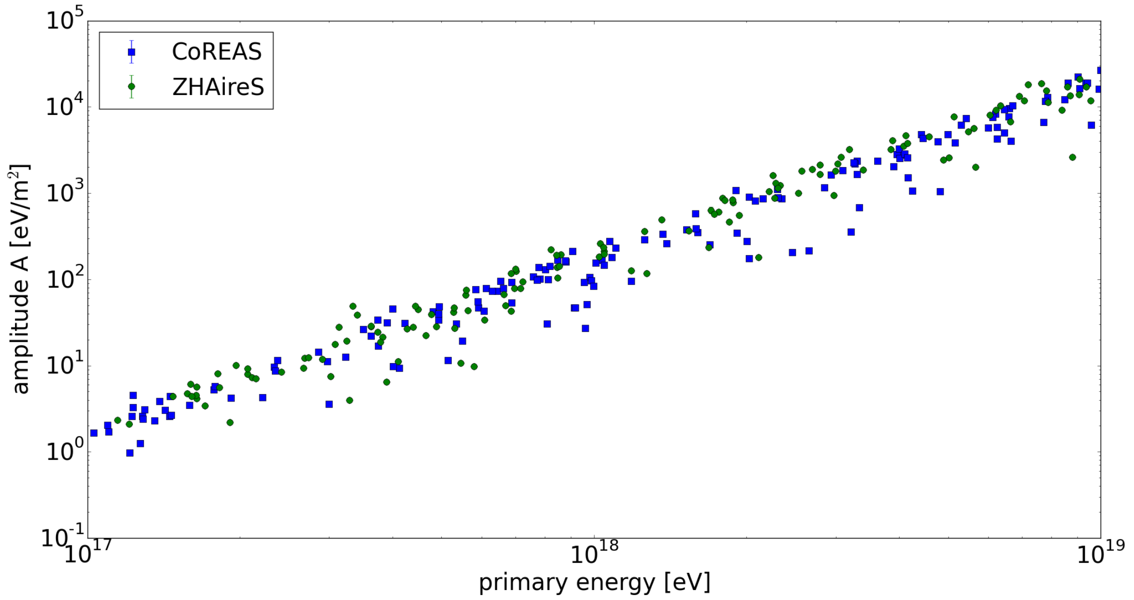

Figure 6.8: Correlation of the amplitude A on the primary energy for CoREAS and ZHAireS.

Applying this reconstruction to the used random showers yields figure 6.9. The ratio between the reconstructed energy E_{recon} and the true value of the Monte Carlo simulations E_{MC} is shown for the mean constants C_i and the combined correction parameters for S_{RD}. The uncertainty is dominated by the uncertainties of the LDF fit.

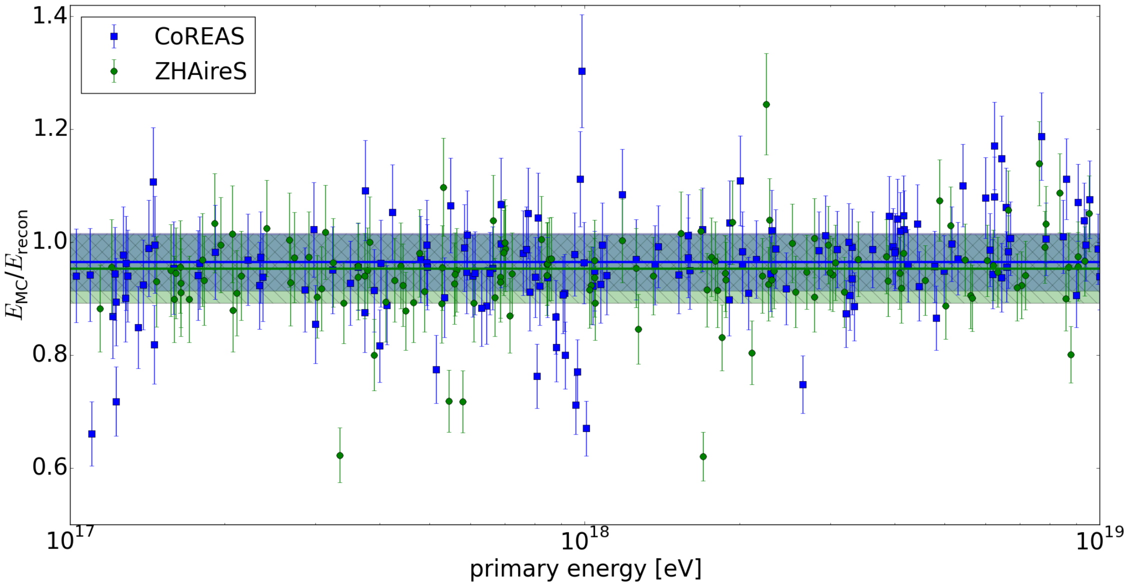

Figure 6.9: Comparison of the reconstructed energy E_{recon} and the true Monte Carlo energy E_{MC}. The mean value and the standard derivation are shown by the solid line and the colored band for CoREAS and ZHAireS.

Mean value and standard derivation are shown by the solid line and the colored band in the figure. For CoREAS (ZHAireS) the mean value is 0.96 (0.95) with a standard derivation of 0.10 (0.12).

On average the energy is overestimated by ≈ 5 % in the reconstruction. The outliers correspond to showers with a lower $\sin(\alpha)$ and higher zenith angle. No bias on the primary energy can be observed. For CoREAS the mean value and the uncertainty of the mean is 0.965 ± 0.008 and 0.95 ± 0.01 for ZHAireS. The standard derivations are 0.10 (CoREAS) and 0.12 (ZHAireS). Thus, the results are consistent within the uncertainty of the mean values.

7 Conclusion

In this thesis the radio emission of extensive air showers has been studied in detail. An efficient method to extract the radiation energy using CoREAS and ZHAireS simulation has been presented. For simulation it is sufficient to place a small number of antennas on the $\vec{v} \times (\vec{v} \times \vec{B})$ arm in the shower plane. Then the radiation energy can be computed with an integration of the energy fluence on that arm.

The influence of the assumption needed for the method have been analyzed. They result in an overestimation of 1.6 % compared to a numerical integration of the interpolation of the two dimensional lateral distribution function. This effect is taken into account by reducing the radiation energy.

The impact of technical parameters in the simulations was analyzed as well. A small thinning level has been found to be enough for this study. This reduces the computing time for the simulation enormously. It was also found the the hadronic interaction model has no relevant influence on the radiation energy.

The method allows to decompose the radiation into the part originating from the geomagnetic emission and the charge excess. It has been found that their ratio, the charge excess fraction, depends on the density at the shower maximum as most of the radiation is emitted close to the shower maximum.

Corrections for the radiation energy have been presented that remove the dependencies of the shower direction and the shower maximum. It has been found that the corrected radiation energy correlates best with the electromagnetic energy of the shower. For an exponential scaling of the refractive index the correlation can be expressed as a quadratic power law. For the comparison of proton and iron primaries a difference of 4 % has been observed. The scatter was found to be around 7 %. With the differences between the CoREAS and ZHAireS code the systematic uncertainty has been estimated at 3 %. This corresponds to 3.5 % statistical and 1.5 % systematic uncertainty of the electromagnetic energy which is well below current experimental limits.

A more practical parametrization without using information about the shower maximum has been given. This increases the uncertainties only slightly to 7.6 % statistical and 3.4 % systematic

The influence of the magnetic field has been studied. The corrections have been extended to incorporate this effect for all relevant magnetic field strengths on Earth. Additionally the effect of the air refractivity has been analyzed. For the realistic range of around ±5 % at the Pierre Auger Observatory a change of 3.5 % in the radiation energy was found.

In a measurement the radiation energy is determined via a fit of the LDF. Since some of the parameters are correlated or too small compared to the current accuracy of radio detectors the number of free parameters can be reduced or replaced by constants. These constants have been estimated for CoREAS and ZHAireS and have been compared with reference values. It has been found that the parametrization depends on several physical quantities and no direct comparison is possible. The comparison of CoREAS and ZHAireS have shown consistent results for the mean values per zenith bin. The difference is usually less than 15 %, for the highest zenith bin it increases to 40 % for one constant. But this is still in agreement within the standard derivation.

With the found constants the LDF has been fitted to simulated events. The primary energy has been estimated using the integral of the LDF and the correlation between corrected radiation energy and the electromagnetic energy. An overestimation of 5 % has been observed. The results of CoREAS and ZHAireS are coincident within the uncertainty of the mean value.

The comparison of CoREAS and ZHAireS show that the shower development and the radio emission is well understood. One can conclude that the implementation of the radio emission is consistent for both codes and that the radio emission of extensive air showers is a well suited estimator of the cosmic ray energy.

References

[1] H. Schoorlemmer. *Tuning in on cosmic rays. Polarization of radio signals from air showers as a probe of emission mechanisms*. PhD thesis. Nijmegen U., 2012. URL: http://inspirehep.net/record/1186117/files/thesis_HarmSchoorlemmer.pdf.

[2] H. Falcke et al. *Detection and imaging of atmospheric radio flashes from cosmic ray air showers*. Nature 435 (2005), pp. 313–316. DOI: 10.1038/nature03614. arXiv: astro-ph/0505383 [astro-ph].

[3] O. Ravel. *The CODALEMA experiment*. Nuclear Instruments and Methods in Physics Research Section A: Accelerators, Spectrometers, Detectors and Associated Equipment 662, Supplement 1 (2012). 4th International workshop on Acoustic and Radio EeV Neutrino detection Activities, S89–S94. ISSN: 0168-9002. DOI: http://dx.doi.org/10.1016/j.nima.2010.12.057. URL: http://www.sciencedirect.com/science/article/pii/S0168900210027981.

[4] T. P. A. Collaboration. *The Pierre Auger Cosmic Ray Observatory*. Nuclear Instruments and Methods in Physics Research Section A: Accelerators, Spectrometers, Detectors and Associated Equipment 798 (2015), pp. 172–213. ISSN: 0168-9002. DOI: http://dx.doi.org/10.1016/j.nima.2015.06.058. URL: http://www.sciencedirect.com/science/article/pii/S0168900215008086.

[5] J. Hörandel. *Radio detection of Cosmic Rays with LOFAR*. PoS ICRC2015 (2016), p. 033.

[6] P. Bezyazeekov et al. *Measurement of cosmic-ray air showers with the Tunka Radio Extension (Tunka-Rex)*. Nuclear Instruments and Methods in Physics Research Section A: Accelerators, Spectrometers, Detectors and Associated Equipment 802 (2015), pp. 89–96. ISSN: 0168-9002. DOI: http://dx.doi.org/10.1016/j.nima.2015.08.061. URL: http://www.sciencedirect.com/science/article/pii/S0168900215010256.

[7] F. G. Schröder. *Radio detection of high-energy cosmic rays with the Auger Engineering Radio Array*. Nucl. Instrum. Meth. A824 (2016), pp. 648–651. DOI: 10.1016/j.nima.2015.08.047. arXiv: 1601.00462 [astro-ph.IM].

[8] D. Heck et al. *CORSIKA: A Monte Carlo code to simulate extensive air showers* (1998).

[9] S. J. Sciutto. *AIRES: A System for air shower simulations. User's guide and reference manual. Version 2.2.0* (1999). arXiv: astro-ph/9911331 [astro-ph].

[10] T. Huege, M. Ludwig, and C.W. James. *Simulating radio emission from air showers with CoREAS*. AIP Conf. Proc. (2013), pp. 128–132. URL: http://dx.doi.org/10.1063/1.4807534.

[11] J. Alvarez-Muñiz, W. R. C. Jr., and E. Zas. *Monte Carlo simulations of radio pulses in atmospheric showers using ZHAireS*. Astroparticle Physics 35.6 (2012), pp. 325–341. ISSN: 0927-6505. DOI: http://dx.doi.org/10.1016/j.astropartphys.2011.10.005. URL: http://www.sciencedirect.com/science/article/pii/S0927650511001927.

[12] C. Glaser et al. *Simulation of Radiation Energy Release in Air Showers*. JCAP 1609 (2016), p. 024. DOI: 10.1088/1475-7516/2016/09/024. arXiv: 1606.01641 [astro-ph.HE].

[13] A. Aab et al. *The Pierre Auger Observatory: Contributions to the 33rd International Cosmic Ray Conference (ICRC 2013)*. In *Proceedings, 33rd International Cosmic Ray Conference (ICRC2013): Rio de Janeiro, Brazil, July 2-9, 2013*. 2013, pp. 11–14. arXiv: 1307.5059 [astro-ph.HE]. URL: http://lss.fnal.gov/archive/2013/conf/fermilab-conf-13-285-ad-ae-cd-td.pdf.

[14] E.-J. Ahn et al. *Cosmic ray interaction event generator SIBYLL 2.1*. Phys. Rev. D80 (2009), p. 094003. DOI: 10.1103/PhysRevD.80.094003. arXiv: 0906.4113 [hep-ph].

[15] G. Battistoni et al. *The FLUKA code: description and benchmarking*. AIP Conf. Proc. (2007), pp. 31–49. URL: http://dx.doi.org/10.1063/1.2720455.

[16] M. Bleicher et al. *Relativistic hadron-hadron collisions in the ultra-relativistic quantum molecular dynamics model*. Journal of Physics G: Nuclear and Particle Physics 25.9 (1999), p. 1859. URL: http://stacks.iop.org/0954-3899/25/i=9/a=308.

[17] J. Alvarez-Muñiz, W. R. Carvalho, and E. Zas. *Monte Carlo simulations of radio pulses in atmospheric showers using ZHAireS*. Astroparticle Physics 35 (Jan. 2012), pp. 325–341. DOI: 10.1016/j.astropartphys.2011.10.005. arXiv: 1107.1189 [astro-ph.HE].

[18] M. D. Domenico et al. *Reinterpreting the development of extensive air showers initiated by nuclei and photons*. Journal of Cosmology and Astroparticle Physics 2013.07 (2013), p. 050. URL: http://stacks.iop.org/1475-7516/2013/i=07/a=050.

[19] C. Glaser. *Thesis in preparation*. PhD thesis. RWTH Aacchen, 2016.

[20] A. Nelles et al. *A parameterization for the radio emission of air showers as predicted by CoREAS simulations and applied to LOFAR measurements*. Astropart. Phys. 60 (2015), pp. 13–24. DOI: 10.1016/j.astropartphys.2014.05.001. arXiv: 1402.2872 [astro-ph.HE].

[21] A. Aab et al. *Energy Estimation of Cosmic Rays with the Engineering Radio Array of the Pierre Auger Observatory.* Phys. Rev. D93.12 (2016), p. 122005. DOI: `10.1103/PhysRevD.93.122005`. arXiv: `1508.04267 [astro-ph.HE]`.

STATUTORY DECLARATION

I certify that I have written the thesis independently myself, using only the sources and aids documented therein, and that I have indicated all quotations as such.